NOVA SCHOOL OF SCIENCE & TECHNOLOGY

DEPARTMENT OF ELECTRICAL AND COMPUTER ENGINEERING

MARTIM AFONSO DE CARVALHO

BSc in Electrical and Computer Engineering

ENHANCED RECEIVERS FOR OFDM SIGNALS WITH SUPER-QAM CONSTELLATIONS

MASTER IN ELECTRICAL AND COMPUTER ENGINEERING

NOVA University Lisbon
March, 2023

NOVA SCHOOL OF SCIENCE & TECHNOLOGY

DEPARTMENT OF ELECTRICAL AND COMPUTER ENGINEERING

ENHANCED RECEIVERS FOR OFDM SIGNALS WITH SUPER-QAM CONSTELLATIONS

MARTIM AFONSO DE CARVALHO

BSc in Electrical and Computer Engineering

Adviser: João Francisco Martinho Lêdo Guerreiro
Assistant Professor, NOVA University Lisbon

Co-adviser: Rui Miguel Henriques Dias Morgado Dinis
Associate Professor with Aggregation, NOVA University Lisbon

Examination Committee

Chair: Filipa Alexandra Moreira Ferrada
Assistant Professor, NOVA University Lisbon

Rapporteur: Paulo Miguel de Araújo Borges Montezuma
Assistant Professor, NOVA University Lisbon

Adviser: João Francisco Martinho Lêdo Guerreiro
Assistant Professor, NOVA University Lisbon

MASTER IN ELECTRICAL AND COMPUTER ENGINEERING

NOVA University Lisbon
March, 2023

Enhanced Receivers for OFDM signals with super-QAM constellations

This document was created with the (pdf/Xe/Lua)LaTeX processor and the NOVAthesis template (v6.9.5) [1].

Acknowledgements

First, I would like to thank my advisor Prof. João Guerreiro and co-advisor Prof. Rui Dinis for the opportunity of developing this dissertation with their enthusiasm, guidance, patience and availability to provide all the help that I asked for. Without them it would not be possible to finish this dissertation.

Additionally, I would like to thank my family for all of their support in this journey.

Abstract

Nowadays, there is a high demand for wireless communication systems with higher throughput. One popular technique widely used in current and developing wireless technologies is Orthogonal Frequency-Division Multiplexing (OFDM) due to its robustness against frequency selective fading and high spectral efficiency. To further extend OFDM capacity to meet the near future's expected demanding needs, OFDM systems with very large Quadrature Amplitude Modulation (QAM) constellations, the so-called super-QAM, are being proposed. However, OFDM signals are prone to nonlinear distortion effects due to their high envelope fluctuations which reduces the system's performance and this issue is aggravated by the increase in the size of the constellation. For the implementation of effective super-QAM OFDM systems, it is crucial to develop receivers that expect and mitigate the nonlinear distortion on the transmitted signal.

In this work, nonlinear distortion on OFDM small QAM and super-QAM constellations signals is studied, along with distortion models and methods to estimate them solely from the transmitted signal, and application of Bussgang noise cancellation receivers and analysis of their performance over a wide range of scenarios.

Keywords: OFDM signals, nonlinear distortion effects, super-QAM, Bussgang Noise Cancellation, estimation of nonlinear distortion models

Resumo

Nos dias de hoje, há uma grande necessidade de criar sistemas de telecomunicação com maior ritmo de dados. Uma técnica popular em tecnologias de telecomunicação atuais e em desenvolvimento é Ortogonal Frequency-Devision Multiplexing (OFDM) devido à sua robustez contra atenuação seletiva na frequência e alta eficiência espectral. Para aumentar ainda mais a capacidade do OFDM de forma a preparar para ritmos ainda mais altos que são expectáveis num futuro próximo, estão a ser propostos sistemas OFDM com enormes constelações de Quadrature Amplitude Modulation (QAM), o chamado super-QAM. O problema é que sinais OFDM são suscetíveis a efeitos de distorção não linear devido às altas flutuações de envolvente e que traz pior desempenho do sistema, sendo esse problema agravado pelo aumento do tamanho da constelação. Para a implementação de sistemas super-QAM OFDM eficazes é crucial desenvolver recetores que mitiguem a distorção não linear no sinal transmitido.

Neste trabalho, estuda-se a distorção não linear em sinais OFDM de pequenas constelações QAM e super-QAM, modelos de distorção e métodos para estimá-los a partir do sinal transmitido, aplicação de recetores de cancelamento de ruído Bussgang e análise de seu desempenho em diversos cenários.

Palavras-chave: Sinais OFDM, efeitos de distorção não linear, super-QAM, Bussgang Noise Cancellation, estimação de modelos de distorção não linear

Contents

List of Figures

List of Algorithms

Acronyms

6G	sixth generation 1, 2
AM/AM	amplitude modulation to amplitude modulation viii, 18–20
AM/PM	amplitude modulation to phase modulation 9, 18, 20
AWGN	additive white Gaussian noise viii, 11–14
BER	bit error rate viii–x, 6, 8–10, 12–14, 17, 23–26, 30–37, 44, 46–54
BNC	Bussgang noise cancellation viii–x, 6, 7, 29, 30, 33–37, 47–52, 54
CCDF	complementary cumulative distribution function ix, 24–26
CP	cyclic prefix 16
DAR	decision-aided reconstruction 7, 8
EHT	extremely high throughput 1
EVM	error vector magnitude ix, 1, 3, 27, 54
FFT	fast Fourier transform 9
GAMP	generalized approximate message passing viii, 13, 14
IBO	input backoff 3
IFFT	inverse fast Fourier transform 17
IOT	internet of things 1
ISI	intersymbol interference 16, 23
MC	multicarrier 2
ML	maximum likelihood 10, 11

NMSE normalized mean squared error x, 43, 47, 48, 54

OFDM orthogonal frequency division multiplexing viii–x, 1–7, 9–13, 15–28, 30, 32, 33, 35–38, 41, 43, 44, 46–51, 53, 54

OOB out-of-band ix, 13, 23, 25, 28

PA power amplifier 2, 3, 5, 6, 8, 9, 13, 15, 17, 18, 22–24, 28, 30, 31, 33, 39, 40, 53, 54

PAPR peak to average power ratio ix, 3, 5, 24–28, 49, 53, 54

PDF probability density function ix, 22, 23, 38, 39, 54

PSD power spectral density 17

PSK phase-shift keying 17

QAM quadrature amplitude modulation viii–x, 2–4, 6, 7, 10, 11, 15, 17, 21–28, 31, 46, 48–54

RF radio frequency 1, 23

RMS root mean square 27

SEL soft envelope limiter viii–x, 18, 19, 21, 24, 25, 31, 36, 38, 39, 49

SNR signal to noise ratio viii–x, 5, 6, 10, 32, 38, 39, 41, 43, 45, 46, 54

SSPA solid state power amplifier viii, x, 19, 20, 40, 41, 44, 45, 47, 48

TWTA travelling wave tube amplifier 9, 19

1 Introduction

1.1 Objectives

The main goal of this work is to conduct research on improved orthogonal frequency division multiplexing (OFDM) receivers that are aware of the distortion effects caused by the saturation of the signal at the amplifier stage of the transmitter. These receivers should be able to operate with strict error vector magnitude (EVM) requirements even for systems employing large constellations, which is a critical aspect in the upcoming sixth generation (6G) communications.

1.2 Motivation

The ever-increasing processing power of electronic devices capable of consuming and generating larger amounts of data than ever before promotes the development of applications of higher-fidelity, namely the recording and streaming of videos that are more faithful to reality. As a consequence, this creates a strong demand for higher data rate communications between devices.

This never-ending yearning for higher data throughput is especially challenging for wireless communication, where many technologies have to share a limited and already heavily populated radio frequency (RF) spectrum. To that end, new technologies are being developed to increase spectrum efficiency and accommodate current and future wireless data rate needs, such as 5G networks, with features like a scalable numerology and flexible spectrum [2], and the amendment standard IEEE 802.11be, also known as Wireless-Fidelity (Wi-Fi) 7, with emphases on extremely high throughput (EHT) [3].

Beyond that, it is foreseeable that the wireless communications challenge will only get tougher: the move beyond personalized communications toward the full realization of the internet of things (IOT) paradigm, the rapid development of data-centric and automated processes, which require a data rates on the order of terabits per second and 10^7 connections per km^2 may exceed the current generation capabilities and so new ideas for the 6G wireless technology are already being proposed [4].

Several issues arise while designing a high data-rate wireless system, such as frequency and time selectivity, multipath propagation and Doppler effect, issues that come from the reflection, diffraction, and scattering of electromagnetic waves in the environment and due to the relative motion between the receiver and the transmitter, which results in decrease of the channel's capacity and poor performance [5].

These complications can usually be mitigated by overpowering the effects of the channel, although this solution is often not viable, specially for mobile devices where energy is a precious resource. This highlights another challenge of wireless communications which is energy efficiency and power consumption, which is considered of tremendous importance for upcoming 6G communications [6].

One popular technique widely used in current and developing wireless technologies is OFDM [2, 3]. Due to its robustness against frequency selective fading, it can deliver a higher data throughput in the same bandwidth than other modulation options such as single-carrier schemes. To further extend OFDM capacity to meet the near future's expected demanding needs, OFDM systems with very large QAM constellations (i.e., the so-called super-QAM) are being proposed. Although, an important drawback of OFDM is its susceptibility to signal distortion at the power amplifier (PA) stage, which can substantially degrade the system's performance [7]. On top of that, using higher-order constellations can exasperate this problem, leading to higher levels of nonlinear distortion. This distortion has both an in-band component that might lead to very poor performance and an out-of-band component, that can compromise the spectral mask containment.

For the implementation of super-QAM OFDM systems it becomes imperative the development of receivers that expect and can mitigate nonlinear distortion effects so that their impact on performance can be reduced.

1.3 Context

It is widely known that the data throughput of a wireless communication system can be augmented by increasing the signal's bandwidth. However, the transmission of wideband signals is challenging due to the multipath propagation phenomenons that lower the effective capacity of the wireless channel. In particular, wideband signals are severely affected by the effect of frequency selective fading which can only be mitigated by complex equalization schemes. To solve this issue, multicarrier (MC) schemes were developed that have lower equalization complexity. This comes from the fact that MC schemes divide the bandwidth into many small bands in which the frequency selective fading effect is negligible, allowing for a simpler individual equalization of each subchannel.

OFDM is a MC scheme that exhibits orthogonality between subchannels, thus the subcarriers can overlap in the frequency domain, which allows better use of the available spectrum, i.e. a high spectral efficiency [7].

Since in the time domain an OFDM signal envelope is a summation of many subcarriers, the corresponding signal envelope presents large fluctuations, which constitutes a

significant drawback relative to single-carrier systems. This effect is noticed in systems with small constellations, but its consequences get more severe when large constellations are employed, which is a natural step that is taken when trying to increase the system's data rate. This is the case of the super-QAM constellations, which are being considered as a promising physical layer enhancement for 6G networks [2].

The envelope fluctuations make OFDM signals highly prone to nonlinear distortion, which can arise from many sources [8]. One of the most typical nonlinearities is associated with signal saturation at the PA stage of the transmitter, which might lead to both in-band distortion and performance degradation, as well as introduce out-of-band signal leakage that might compromise the compliance of the spectral mask [9]. As a consequence, this issue yields a strong trade-off between linearity and energy efficiency. This is explained by the fact that the maximum energy efficiency of the PA is obtained when the input signal is near the PA's saturation point. However, since the OFDM signals have sporadic high peaks, most of the time the PA has to operate at a much lower point (i.e., with a higher input backoff (IBO)) because otherwise the linearity will be compromised [7]. However, the use large IBOs dramatically reduces the energy efficiency of the PA.

There are several peak-to-average power ratio (PAPR) reducing techniques developed to reduce the OFDM envelope fluctuations [10, 11]. However, the most efficient ones involve a simple digital clipping operation, which causes the nonlinear distortion effects.

For these reasons, it is generally unavoidable that OFDM signals are impaired by nonlinearities, especially on the transmitter side. This prompts the design and investigation of reception techniques able to deal with the distortion effects. In the literature, one can find several ways to deal with the nonlinear distortion in OFDM signals, which can be generally categorized into three types of approach:

- Consider it as noise that is added to the receiver noise while using a conventional OFDM receiver. As a consequence, considerable performance degradation can take place.

- Consider it as noise but try to estimate it and cancel it from the received signal. This is the operation of the so-called Bussgang receivers [12].

- Consider it as useful information. This takes advantage of the fact that the nonlinear distortion is a function of the transmitted signals. However, this approach requires sophisticated receivers that might present considerable complexity [13, 14].

This thesis aims to investigate receiver designs for nonlinear OFDM systems with super-QAM constellations. The main goals are to study the EVM requirements for different levels of performance, as well the development of reception schemes able to operate with low EVM, while not sacrificing the achievable performance.

1.4 Organization

This thesis is organized as follows: In chapter 2 is presented the state of the art of OFDM receivers. It is discussed how each receiver interprets or mitigates the distortion of the received signal and what additional complexity is required for its implementation when compared to a conventional receiver. In chapter 3, OFDM systems and distortion models are characterized, the drawback of a system without any distortion compensation technique is understood and so is the aggravation of the drawback for systems with super-QAM constellations, and metrics for comparison of compensation techniques are introduced. In chapter 4 the Bussgang noise cancellation receiver introduced in chapter 2 is studied in depth, and two algorithms for estimation of distortion model parameters are presented. This receiver performance is analyzed for 16-QAM and super-QAM. Finally, chapter 5 resumes this thesis and presents perspectives for future work.

2

State of The Art

High PAPR is a characteristic of OFDM signals that makes it susceptible to saturation at the PA stage of the transmitter. This nonlinear distortion effect can be deliberately applied to the signal in order to increase the energy efficiency of the system or can happen naturally during the transmission of the signal as a known occurrence and accepted imperfection of the system. Either way, nonlinear distortion always happens to some extent in OFDM signals and it's up to the receiver side to estimate the transmitted signal while accepting the distortion as noise or by acknowledging that the distortion of the received signal is dependent on the original signal and thus recognize it as a component of the signal, i.e. use it as useful information.

In order to benefit from the greater energy efficiency provided by nonlinear OFDM without a considerable performance penalty, receivers that are aware of the characteristics of the distortion operation should be considered.

This chapter contains the state of the art of OFDM receivers and is divided in three sections, where each section gathers the receivers that view the distortion component of the received signal in a similar way: in section 2.1 the distortion is viewed as a component indistinct from channel noise. In section 2.2 the distortion is to be estimated and removed. In section 2.3 the distortion is expected as a valid part of the signal modulation.

2.1 Conventional Receivers

A conventional OFDM receiver perceives nonlinear distortion as a component uncorrelated to the transmitted signal and so estimates the signal as if the distortion was noise added by the wireless channel and thus the signal degradation is not mitigated.

The estimation of the original transmitted signal from the received one is done after channel equalization by a hard decision demodulator without any processing of the signal and thus the best case scenario is where the effect of the distortion plus the noise of the channel does not displace the signal constellation points into the region of neighbouring constellation points. As a consequence the SNR of the transmission has to be tighter.

Another unfortunate characteristic of a nonlinear distorted signal is that it tends to

have its constellation contract to the center as if it was scaled down. This has massive impact on the effectiveness of the hard decision demodulator for constellations larger than 4-QAM because points of the constellation further away from the origin experience large migrations towards the origin. Although on a real implementation of an OFDM system this may not be noticed as the signal is amplified at the receiver's low-noise amplifier and thus mitigates the scaling down of the nonlinear distortion.

2.2 Distortion-aware Receivers

2.2.1 Bussgang Noise Cancellation

OFDM signals distorted by a nonlinear operation can be decomposed into a useful component proportional to the original signal and an uncorrelated nonlinear distortion component, as described by the Bussgang's theorem [15]. Since the nonlinear distortion behaves as an additional noise-like term, it leads to performance degradation of the OFDM system.

Bussgang noise cancellation (BNC) receivers, also known as Bussgang receivers, are receivers that treat the nonlinear distortion term from Bussgang's theorem as a signal to be estimated and subsequently removed. The BNC algorithm assumes that most of the estimation done by the traditional QAM demodulator is correct and tries to compensate the distortion by re-modulating the estimated symbol, passing it trough the same nonlinear distortion as in the transmitter power amplifier, and then subtract from the original received signal the difference between the re-modulated and distorted signal. This iterative process is presented in algorithm 1.

Algorithm 1: BNC algorithm.

1: Received symbol is demodulated by a hard decision demodulator which assumes all distortion as channel noise.
2: Symbol is modulated again but without the assumed channel noise.
3: Modulated symbol is nonlinear distorted by a model of the transmitter's power amplifier.
4: Difference between the modulated symbol before and after the distortion operation is the estimated distortion component.
5: Estimated distortion component is removed from the received symbol and algorithm jumps back to step 1.

The performance of these receivers considering the ideal case of known nonlinearity parameters is shown in figure 2.1. From the figure, it can be observed that with the increase of the number of iterations, the BER curve of the BNC receiver gets closer to the BER curve of an equivalent linear OFDM system (i.e. OFDM with an ideal PA) . In this example it is unable to correct all the bit-errors and from step two to three it makes it worse by estimating inaccurate noise.

A drawback with this type of receiver is that the estimation of the nonlinear distortion is difficult, especially at low SNR where each iteration results in more signal degradation

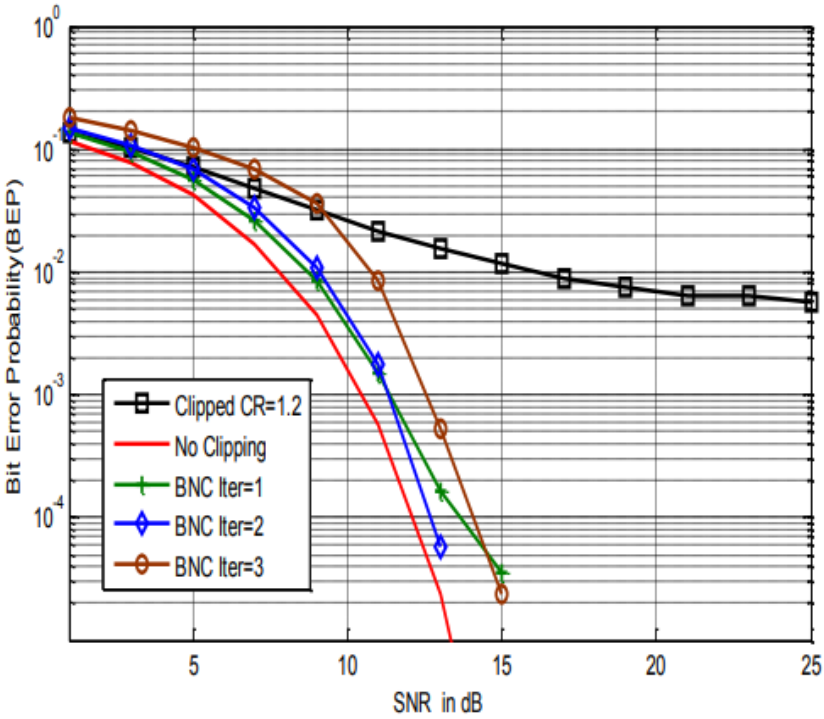

Figure 2.1: Performance of BNC algorithm. Clipping ratio of nonlinear distortion $CR = 1.2$, 16-QAM, 64 subcarriers [12].

[16].

BNC receivers are studied in more detail in chapter 4.

2.2.2 Decision-Aided Reconstruction

Decision-aided reconstruction (DAR) is an iterative technique that assumes that parts of the received signal with power below the saturation threshold of the distortion operation are equal to the signal received from an equivalent linear OFDM transmitter. All signal with power near or above the saturation level is discarded and replaced by an estimation. By repeating this process multiple times, the parts of the signal above the distortion threshold grow back to the original linear signal. Algorithm 2 presents this process step-by-step.

Algorithm 2: DAR algorithm.

1: Received symbol is demodulated by a hard decision demodulator which assumes all distortion as channel noise.
2: The symbol is modulated again but without the assumed channel noise.
3: Points of the modulated symbol with magnitude in the linear region of the transmitter's power amplifier are replaced by the received symbol.
5: The resulting symbol is set as the received symbol for the next iteration of the algorithm.

In figure 2.2, the performance of a DAR receiver is presented. The receiver improves the

BER of the nonlinear system, although has a large performance difference when compared to a linear system. This can be explained by the fact that the wireless channel adds noise to the signal and thus perfect equalization is impossible, in the decoder the high-power parts of the signal that will be replaced completely depend on the rest of the signal that is assumed to be linear, but because of distortion introduced by the channel the degradation is propagated from the low to the high-power sections during the reconstruction process.

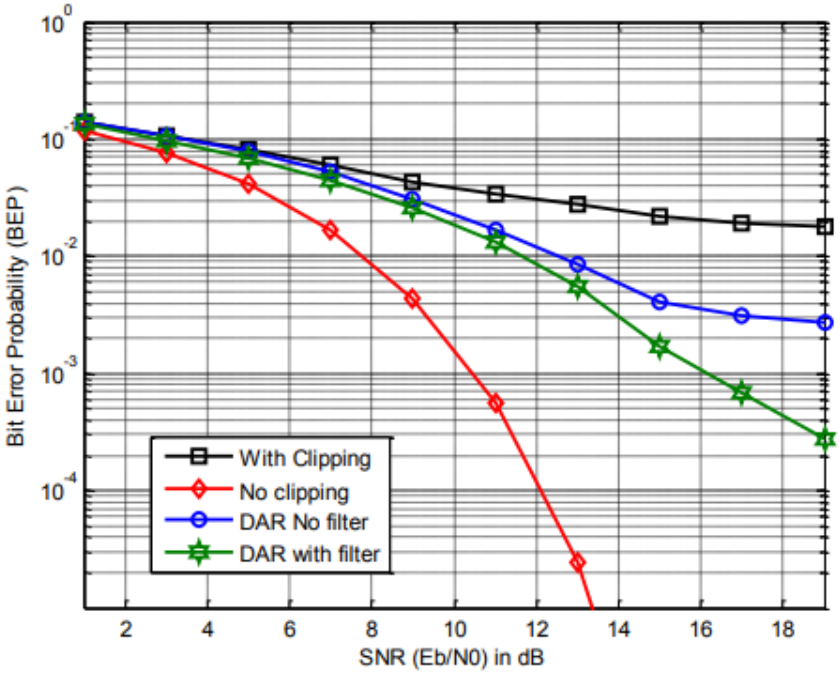

Figure 2.2: Comparison of the modified DAR with the original form of DAR, N=64, CR=1.2, Iteration=3 [12]

In [17] is presented a similar technique based on the same principle as DAR, as it assumes certain parts of the signal in time domain as true and doesn't try to correct them, but which additionally does the same thing for the frequency domain.

At the output of the PA, the signal can be segmented and grouped into two groups: The low-power symbols that are little affected by the transmitter's nonlinear distortion, named x_t, and the rest that have high power and are out of the linear zone, named x_f. Thus the distorted signal in time domain, $x[n]$, can be written as

$$x = \begin{bmatrix} x_f \\ x_t \end{bmatrix}, \tag{2.1}$$

where x_f are the points of the signal that will be replaced during the symbol reconstruction. Similar separation is done on the signal in the frequency domain where points are considered to be reliable and thus grouped in X^t_{est} if positioned near a point of the constellation. In order to do that, the system of linear equations, which is presented below, when solved for the points that are assumed as incorrect (thus points that are treated as unknown variables), gives the original non-distorted signal.

At the receiver, the time-domain signal is passed through a fast Fourier transform (FFT) to convert it into frequency-domain. This can be expressed in matrix form as

$$X = FFT(x) = Wx \Leftrightarrow \begin{bmatrix} X_{est}^{t} \\ X_{est}^{f} \end{bmatrix} = \begin{bmatrix} G & F \\ E & D \end{bmatrix} \begin{bmatrix} x_f \\ x_t \end{bmatrix}, \tag{2.2}$$

where X represents x in the frequency domain, both X and x are vectors with size of number of subcarriers, and D, E, F and G are sub-matrices of the discrete Fourier transform matrix.

The values of the high power segments of the signal can be found by solving the system of equations where x_f is treated as an unknown and X_{est}^{t} is the reliable constellation point. The solution is expressed by

$$X_{est}^{t} = Gx_f + Fx_t \Leftrightarrow x_f = G^{-1}(x_{est}^{t} - Fx_t). \tag{2.3}$$

This equation is solvable if the length of vector x_f is less than the length of vector x_{est}^{t}. The steps of this method can be found in algorithm 3.

Algorithm 3: Reconstruct receiver algorithm.

1: Received symbol x is demodulated by a hard decision demodulator into X_{est}.
2: Symbol is modulated again into x_h.
3: Locate the correctly estimated symbols X_{est}^{t} by identifying the values close to zero in $FFT(x - x_h)$.
4: Locate symbols with power levels inside the linear region of the PA and group them into x^t.
5: Through equation 2.3, compute x^f.
6: Joining x^t and x^f and positioning them at the correct indices then x_est is obtained.

Figure 2.3 presents the BER of this type of receiver using two configurations of travelling wave tube amplifier (TWTA) models with different intensities of amplitude modulation to phase modulation (AM/PM) distortion, definition of these models can be found in section 3.2.1. Figure 2.4 shows the same but for OFDM systems with harsher nonlinearity requirements, the larger constellation size worsens the BER by a factor of almost 10^5.

2.3 Distortion-aided Receivers

2.3.1 Optimum and Sub-optimum Receivers

The OFDM receivers presented in the previous section try to cancel the distortion component from the received signal and in doing so obtain its original linear signal. These receivers choose to discard the nonlinear part because it is seen as an uncorrelated component to the original signal, but in fact the nonlinear distortion component is a function of the input signal, and thus correlated, and that means that it can be helpful when estimating the original signal. [18].

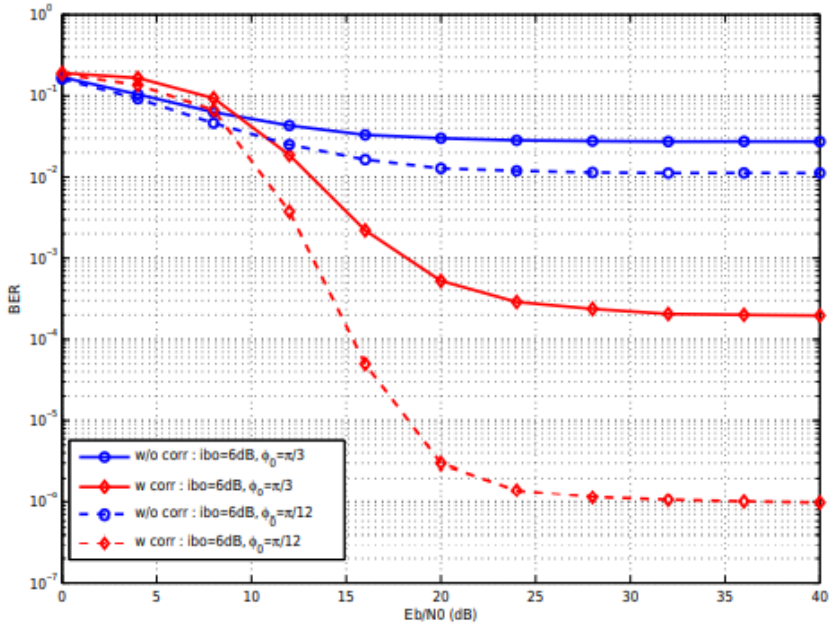

Figure 2.3: BER vs SNR for 16-QAM, 256 subcarriers. [17]

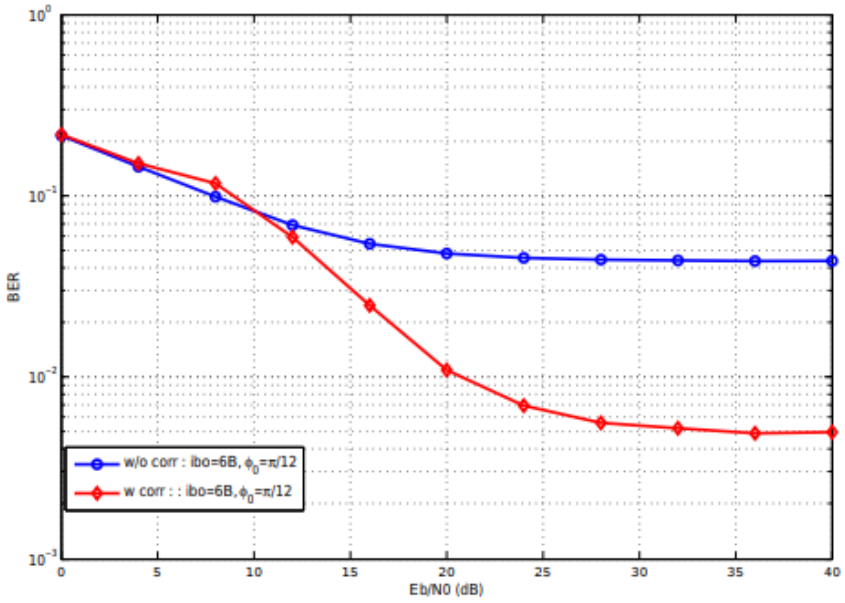

Figure 2.4: BER vs SNR for 64-QAM and 256 subcarriers. [17]

The optimum receiver is the maximum likelihood (ML) receiver where the received symbol is compared to all possible transmitted OFDM symbols and the one with the smallest Euclidean distance to the received symbol is selected (as presented in algorithm 4) . In doing so, the receiver takes into account the full signal to make its decisions, including the high-power distorted parts.

In [18] it is shown that the ML receiver can even outperform linear OFDM transmitters. In other words, it is demonstrated that the presence of nonlinear distortion in the signal can decrease the BER instead of increasing it, which is a surprising result.

Algorithm 4: ML algorithm.
Iterate through all possible symbols that the OFDM system can produce, apply the nonlinear distortion, and chose the symbol with the smallest Euclidean distance to the received signal.

However, the implementation complexity of a ML receiver is prohibitively high. For example, for a 16-QAM OFDM system with 128 subcarriers, the receiver has to do $16^{128} \approx 10^{154}$ symbols comparisons for performing a single decision. Therefore, even for a smaller number of subcarriers, this remains an issue.

Optimum receivers promise equal or better performance than conventional linear OFDM systems, but their implementation is prohibitively complex even for systems with a small number of subcarriers and small constellation. Thus, to achieve the ML gains to a smaller degree, sub-optimal receivers have been developed that run the ML algorithm, but on smaller sets of sequences [18].

In article [18] it is shown that on symbols that differ in one bit, harsher distortions increase the minimum Euclidean distance between any two symbols of that set (asymptotic gain is proportional to the minimum Euclidean distance squared between two symbols). A higher distance between symbols means that the decoder can decide with more certainty. In other words, a signal with high nonlinear distortion where the channel-induced distortion switches one bit has a higher chance of being corrected by an optimal receiver than if the nonlinear distortion was lower. Also, the Euclidean distance tends to increase linearly with the number of switched bits. The gain increased linearly with the number of modified bits, suggesting that the conclusions for uncoded OFDM also apply to coded OFDM schemes. These tendencies of an optimum receiver are even higher for frequency-selective channels than the ones presented in the figures with an ideal AWGN channel [18].

Four sub-optimal receivers algorithms and associated performance are presented in [18] with different methods to select received symbol bits in order to flip them and compare resulting Euclidean distances. If the optimal symbol differs from the hard decision symbol in a small number of bits, by testing only a small fraction of all possible sequences there is a high chance that the optimal sequence is among them [18]. Algorithms in 5 describe possible implementations of sub-optimum receivers.

Method I produces an acceptable performance for small values of L_b, as seen in figure 2.5, but its performance degrades substantially when the number of subcarriers increases. Method I is also used in the receiver proposed in [19].

Switching only one bit, as in method II with the performance presented in figure 2.6, results in an unsatisfactory performance when compared to an optimum receiver. On the other hand, method III gives great results, better than linear OFDM transmissions, the downside is that its complexity increases linearly with the number of subcarriers.

Method IV is a variant of method III with the objective of reducing the receiver complexity.

Algorithm 5: Sub-Optimal Receivers

Method I - Select the Lb bits where the hard decision decoded received signal is closer to the decision threshold, iterate through all possible symbols that the OFDM system can produce by varying those Lb bits, apply the nonlinear distortion, and choose the symbol with the smallest Euclidean distance to the received signal.

Method II - Produce all variations of the hard decision decoded received signal by only switching one bit, apply the nonlinear distortion, and chose the symbol with the smallest Euclidean distance to the received signal.

Method III - Iterate through the hard decision decoded received signal bits and switch them if the resulting signal, after the nonlinear distortion, has a smaller Euclidean distance to the received signal. Repeat the procedure until no smaller Euclidean distance is found.

Method IV - Iterate through the hard decision decoded received signal P bits closer to the decision threshold and switch them if the resulting signal, after the nonlinear distortion, has a smaller Euclidean distance to the received signal. Repeat the procedure until no smaller Euclidean distance is found.

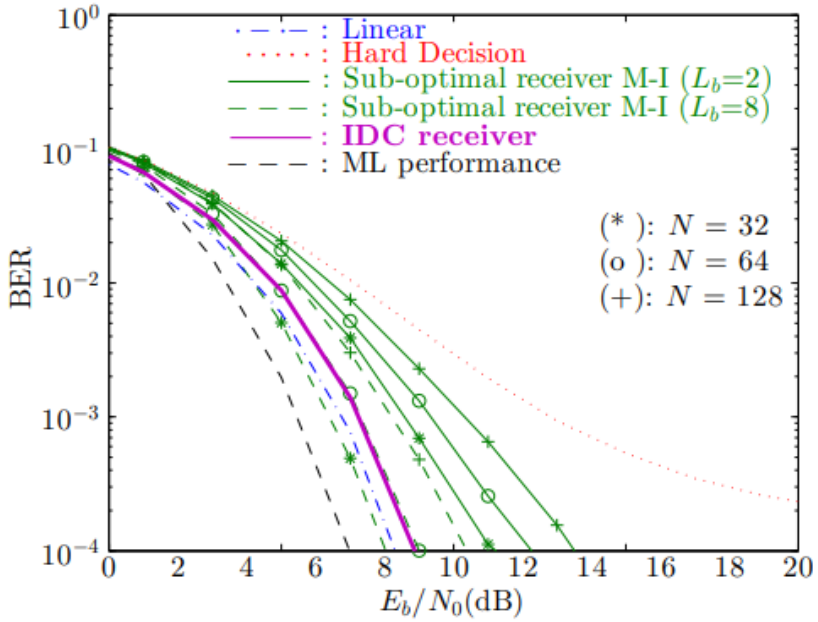

Figure 2.5: BER performance for method I in an ideal AWGN channel. [18].

In [18] is shown that method IV has good performance but not as good as method III.

2.3.2 Belief Propagation Receivers

Sub-optimum receivers presented in previous section fall far from the optimum performance and their complexity is still high [16].

The model of a received nonlinear OFDM signal in an ideal AWGN channel can be expressed as

$$y_n = f(s_n) + w_n, \tag{2.4}$$

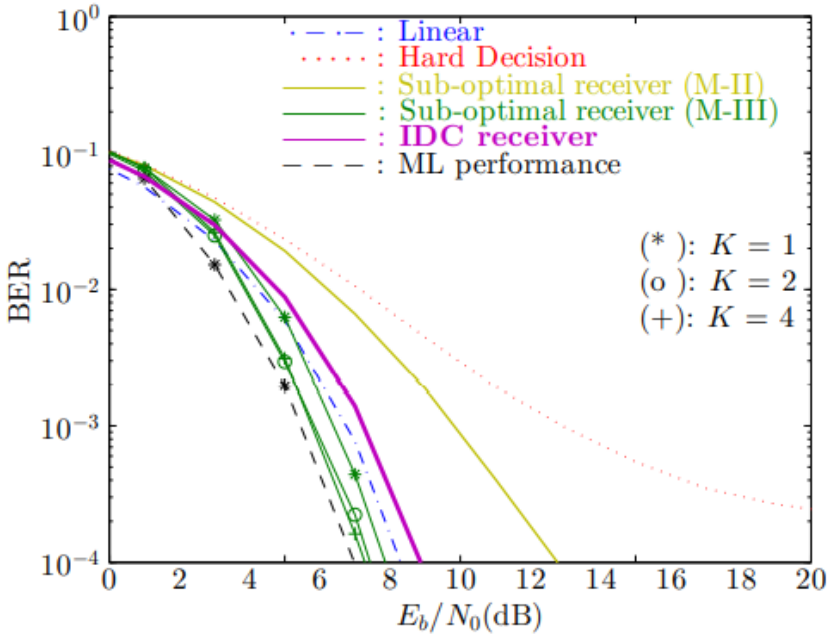

Figure 2.6: BER performance for methods II and III in an ideal AWGN channel. [18].

where w_n is white Gaussian noise, s_n is the linear OFDM signal and f is the nonlinear distortion applied by the transmitter's PA. This model is equivalent to a general problem statement for the generralized approximate message passing (GAMP) algorithm, which belongs to a class of Gaussian approximations of loopy belief propagation for dense graphs. It is used the sum-product variant of the GAMP algorithm that approximates the minimum mean-squared error estimates of s_n. [20]

The GAMP receiver performance is presented in figure 2.7. As shown, the achievable BER performance can be significantly better than that of the linear OFDM. Application of OOB filter degrades the performance but that is to be expected as the receiver is designed assuming that there is no OOB filtering and the filtering operation itself removes information from the signal. A Nyquist rate (with no oversampling) version of the receiver has no spectral regrowth issues because all nonlinear distortion components fall in-band [16].

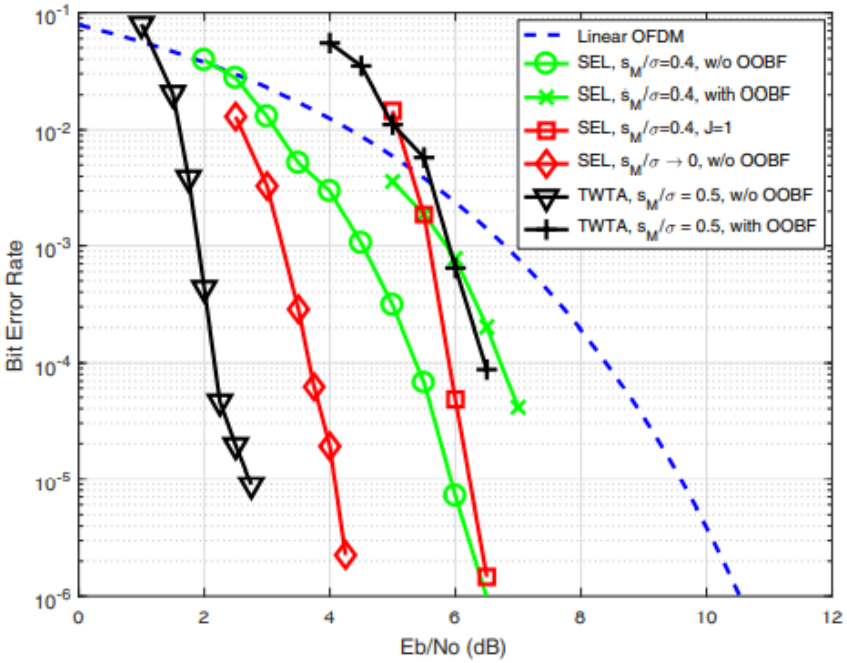

Figure 2.7: BER performance for an ideal AWGN channel with considering the GAMP receiver of [16].

3

Nonlinear OFDM

This chapter is dedicated to the characterization of nonlinear OFDM schemes with emphasis on the nonlinear distortion effects on performance. The chapter starts with an introduction of OFDM modulation and the improvements that it can bring to a wireless system, followed by the unfavorable impact that the transmitter's PA nonlinear behaviour has on that modulation, which is studied with the characterization of nonlinear OFDM systems and models that describe the PA distortion. The effects of the distortion are analyzed and it is determined why OFDM signals are prone to distortion. After that the ramifications of the nonlinearity on systems with Super-QAM constellations is observed, and finally metrics are introduced in order to measure and compare methods that mitigate the PA's nonlinear characteristics, such as the ones introduced in the previous chapter or those that will be studied in chapter 4.

This chapter is organized as follows: in section 3.2 the characterization of an OFDM system is presented along with models for the non-ideal PA. Section 3.3 denotes the negative effects of the PA distortion on a OFDM signal with emphasis on systems with large constellations. Section

3.1 Metrics

introduces metrics to compare the performance of techniques to deal with the inherent OFDM nonlinearity.

3.2 System Characterization

OFDM is a multicarrier technique that divides a stream of digital data into multiple sub-streams that are modulated and uniformly distributed in frequency, each sub-stream is modulated into a subcarrier. The fundamental idea behind OFDM is an evolution of the traditional frequency-division multiplexing schemes.

In OFDM, the subcarriers are synchronized and send information concurrently in bursts, also known as OFDM symbols or OFDM blocks, where during the period of a

symbol the subcarrier waveform is a pure tone, the information of each subcarrier is modulated in the constant amplitude and phase of the tone.

The intrinsic orthogonality between subcarriers, which is a characteristic of OFDM signals, allows those subcarriers to be tightly packed together in the spectrum without interference and thus, efficient usage of the spectrum can be achieved.

Having a signal partitioned into many subcarriers instead of being wideband as in single carrier schemes [21] it is beneficial to mitigate frequency selective fading, which is associated with the multipath channel effects of the propagation environment. Since for narrow-band signals the frequency selective fading is locally perceived as flat fading, the subcarriers of a multicarrier signal can be individually equalized by a simple linear operation.

Between adjacent OFDM symbols, there is a cyclic prefix (CP) so that the multipath phenomenon's replicas of the signal that arrive at the receiver with different delays do not interfere with the following burst. This particularity of OFDM helps to mitigate the so-called intersymbol interference (ISI). As is widely known, ISI is most noticeable on high data rate communications where symbol periods are small compared to the channel delay spread. In those conditions, the existence of a guard time between consecutive symbols is extremely important. This might be a significant limitation for single carrier techniques, but in contrast, the multicarrier nature of OFDM with its relatively lower data rate of each stream allows for higher overall data rates while achieving lower ISI due to larger symbol duration.

A given baseband OFDM signal, $s(t)$, is defined as a sequence of data bursts spaced by the symbol duration T, as

$$s(t) = \sum_{m} s_m(t - mT)w(t - mT), \tag{3.1}$$

where T denotes the OFDM symbol duration and $s_m(t)$ represents the m^{th} symbol of the OFDM signal, which consists in a repeating signal constricted in a time window by the support pulse $w(t)$. The OFDM signal has its bandwidth uniformly divided into N subcarriers, each one with baseband center frequency at $f_k = K/T$, where k is the index of the subcarrier.

$$s_m(t) = \sum_{k=0}^{N-1} |S_{m,k}| e^{2\pi f_k t + arg(S_{m,k})} = \sum_{k=0}^{N-1} S_{m,k} e^{j2\pi f_k t}, \tag{3.2}$$

where $S_{m,k} = |S_{m,k}| e^{jarg(S_{m,k})}$ represents the complex data symbol selected from a given constellation transmitted on the k^{th} subcarrier of the m^{th} burst.

To keep its orthogonal properties when building the symbol s_m, the spacing between subcarriers is set to match the period T_w of the pulse function $w(t)$. If the pulse is a rectangle function then

$$\mathcal{F}\{s_m(t)w(t)\} = \mathcal{F}\{s_m(t)\} * sinc(\pi f T_w), \tag{3.3}$$

where $\mathcal{F}\{s_m(t)\}$ is a train of diracs.

Figure 3.1 shows the power spectral density (PSD) of an OFDM signal considering 4-QAM OFDM symbol and $N = 8$ subcarriers. It can be observed that the time domain pulse functions overlap in the frequency domain except at the exact subcarrier frequencies, thus the power of the symbol at f_k only contains the power of the k subcarrier.

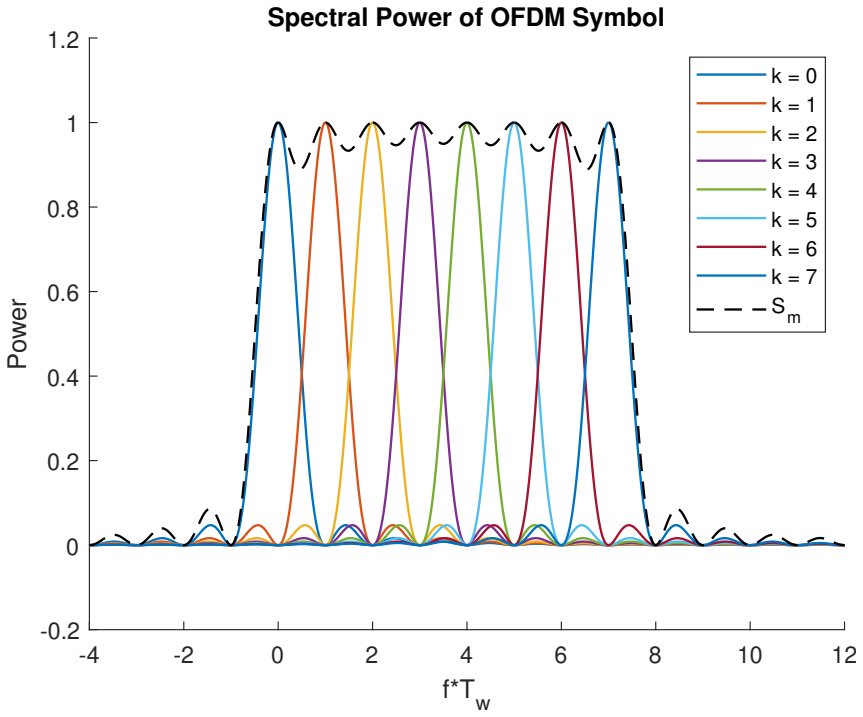

Figure 3.1: Spectral power of a 4-QAM OFDM symbol with $N = 8$ subcarriers.

One important feature of OFDM is that the signals to be transmitted can be modulated and demodulated with the use of discrete Fourier transforms. Essentially, the time-domain samples of a given OFDM signal $\{s_n\}$ can be generated by applying an inverse fast Fourier transform (IFFT) to the block of N complex data symbols $\{S_k\}$. Where each data symbol S_k is a mapped value from a constellation of M points (M-phase-shift keying (PSK) or M-QAM for example).

Nonlinear OFDM is a system where the signal distortion is accepted in order to increase the energy efficiency of the PA. This is accomplished by deliberately clipping the signal or by designing the PA to have an operation point that lies outside the linear region of the amplification characteristic.

Better energy efficiency comes at the cost of signal degradation and spectral broadening. The magnitude of these nonlinear distortion effects depends on the harshness of the nonlinearity (for instance the clipping level, when the signal is deliberately clipped at the transmitter to reduce the envelope fluctuations) and the size of the constellation. A direct consequence of the signal degradation caused by the nonlinear distortion is the increased BER observed at the receiver side. Moreover, spectral broadening can lead to unwanted spectral emissions that compromise the spectral mask.

A block diagram of a complete nonlinear OFDM system is shown in figure 3.2, which includes all three stages: transmitter, channel and receiver. The modulator and demodulator that shifts the signal between baseband and carrier frequency is not included. The essential information to take from this diagram is the order of operations and the symbols given to the signal between operations, which are used throughout this document. Asterisk is used as the convolution operator.

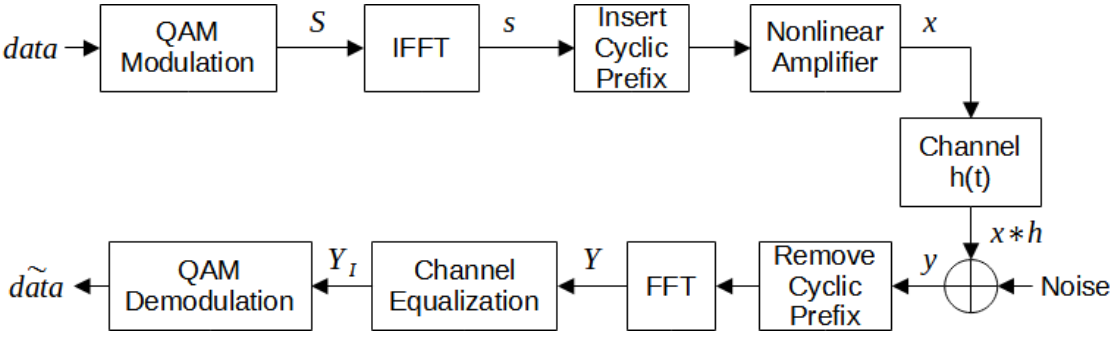

Figure 3.2: Block diagram of nonlinear OFDM system.

3.2.1 Nonlinearity Models

The models of the three most common nonlinearities associated with radio frequency PA used in OFDM systems are given in the following. These models are important for the study of the nonlinear distortion effects and for the estimation of original signal at the receiver by reproduction of the transmitter's nonlinearity.

In this thesis, it is considered the general bandpass model for the PA. This model is generally characterized by the AM/AM conversion function $f_A(|s_n|)$, and the AM/PM function $f_\Theta(|s_n|)$. Notice that both functions depend solely on the input signal's amplitude [12]. Any nonlinear model can be described by defining these two functions. Let us consider a given input OFDM signal and its polar format is given by

$$s_n = |s_n| e^{j arg(s_n)}. \tag{3.4}$$

If this signal is submitted to a nonlinear operation, the distorted signal is expressed as

$$x_n = f(s_n) = f_A(|s_n|) e^{j(f_\Theta(|s_n|) + arg(s_n))}. \tag{3.5}$$

The three most used PA models encountered in the literature are:

- SEL - Soft envelope limiter: also known as clipping, is the most simple nonlinearity operation to model: if the signal amplitude is above the threshold it saturates without any change to the phase. Although not suitable to characterize most amplifiers, by having a single parameter (i.e., the clipping threshold s_M), it is an interesting nonlinear operation to study saturation effects on the signal. Its AM/AM and AM/PM

functions are given by [12]

$$f_A(|s_n|) = \begin{cases} |s_n|, & |s_n| \leq s_M \\ s_M, & |s_n| > s_M \end{cases} \tag{3.6}$$

$$f_\Theta(|s_n|) = 0. \tag{3.7}$$

- SSPA - solid state power amplifier: also known as Rapp's model, is a model for a solid-state amplifier. It contains two parameters denoted by s_M and p. The first one sets the saturation threshold and the other one characterizes the smoothness of the transition between the linear and nonlinear regions. SSPA model is described in [8] by

$$f_A(|s_n|) = \frac{|s_n|}{(1 + (\frac{|s_n|}{s_M})^{2p})^{\frac{1}{2p}}}, \tag{3.8}$$

$$and \tag{3.9}$$

$$f_\Theta(|s_n|) = 0. \tag{3.10}$$

  As parameter p increases, the SSPA model converges to the SEL model.

- TWTA - traveling wave tube amplifier: also known as the Saleh model, is a general approximation of a real amplifier. For a field implementation of a nonlinear OFDM system, this model gives more accurate results than if using the SEL model. TWTA model is expressed as [22]

$$f_A(|s_n|) = \frac{\alpha_A |s_n|}{1 + \beta_A |s_n|^2}, \tag{3.11}$$

$$and \tag{3.12}$$

$$f_\Theta(|s_n|) = \frac{\alpha_\Phi |s_n|^2}{1 + \beta_\Phi |s_n|^2}, \tag{3.13}$$

  where α and β coefficients are extracted from the amplifier's characteristics. In order to compare it with other models and have its saturation at the same threshold, β_A can be calculated as

$$\beta_A = \left(\frac{\alpha_A}{2 s_M}\right)^2. \tag{3.14}$$

Figure 3.3 shows the AM/AM functions of the different bandpass nonlinearity models presented above considering a saturation level of $s_M/\sigma = 0.5$. Unlike SEL model, the TWTA and SSPA models reduce signal amplitudes before the saturation point. As a consequence amplitudes below that threshold will also exhibit some amplitude distortion and in the case of TWTA also phase distortion.

For the rest of this work, the threshold level s_M is described as the ratio from the threshold to the signal's standard deviation, i.e. s_M/σ, where $\mathbb{E}[|s_n|^2] = 2\sigma^2$ is the variance of s_n. This is done so that identical thresholds can be applied to different OFDM signals independently of symbol power or constellation size.

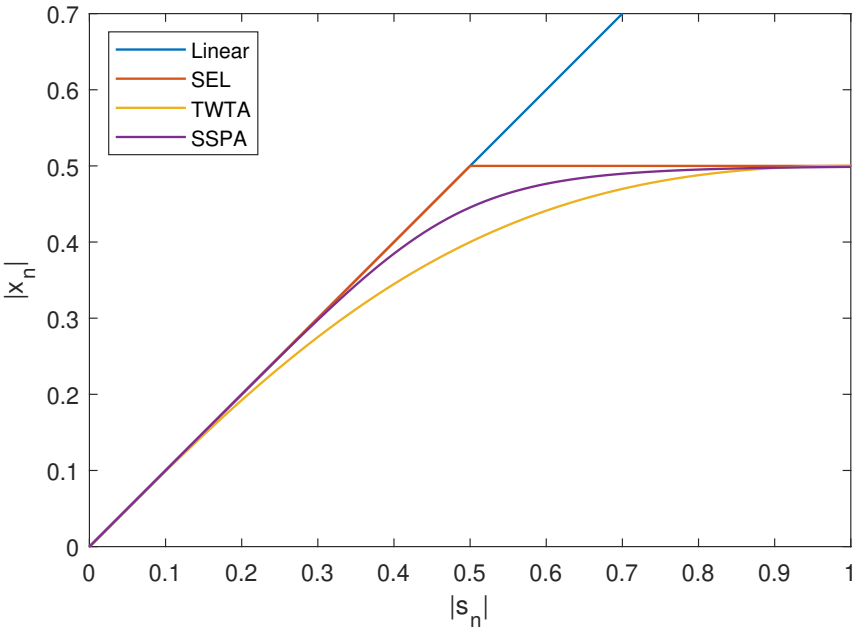

Figure 3.3: AM/AM distortion characteristics of nonlinear amplifiers. Parameter p of SSPA is 3.

3.2.2 Nonlinear Distortion Effects

The signal OFDM signal resulting from a nonlinear distortion operation as the previous ones can be characterized by Bussgang's theorem [15]. Bussgang's theorem states that an application of a nonlinear distortion on a signal with Gaussian distribution results in a signal that can be decomposed as the sum of a "useful" component, proportional to the original signal, and an uncorrelated component. This allows writing the nonlinearly distorted signal as

$$x_n = f(s_n) = \alpha s_n + d_n, \tag{3.15}$$

where α is a complex-valued scale factor and d_n concentrates the nonlinear distortion, being uncorrelated with original samples of OFDM s_n. The scale factor α is a coefficient intrinsic to the AM/AM and AM/PM functions of the nonlinear operation and can be computed by the equality

$$\alpha = \frac{E[x_n s_n^*]}{E[|s_n|^2]} = \frac{\int_0^\infty R f_A(R) e^{i f_\Theta(R)} p(R) dR}{2\sigma^2}, \tag{3.16}$$

where R sweeps through all the magnitudes of the signal, d_n is uncorrelated with s_n, thus $E[d_n s_n] = 0$ and $p(R)$ is the Rayleigh distribution, given by

$$p(R) = \frac{R}{\sigma^2} e^{-\frac{R^2}{2\sigma^2}}, \tag{3.17}$$

with σ^2 denoting the average power of the input signal. Since the signal detection in OFDM is made in the frequency domain, it is useful to define the Busgang's theorem in that domain,

$$X_k = \alpha S_k + D_k, \tag{3.18}$$

where S_k and D_k are the original symbol (i.e, a given constellation point) and the distortion term associated with the k^th subcarrier, respectively.

The linear part of the Bussgang representation, i.e. the scale factor α can be observed in figure 3.4, where it is shown the constellation of OFDM signals impaired by an SEL operation under different clipping levels. It can be observed that the lower the clipping level, the more condensed the signal constellation becomes and thus magnitude of α becomes smaller. The spread of points around the original signal scaled by α is the effect of the nonlinear component d_n. Clearly, the size of this "cloud"of points increases with the severity of the clipping.

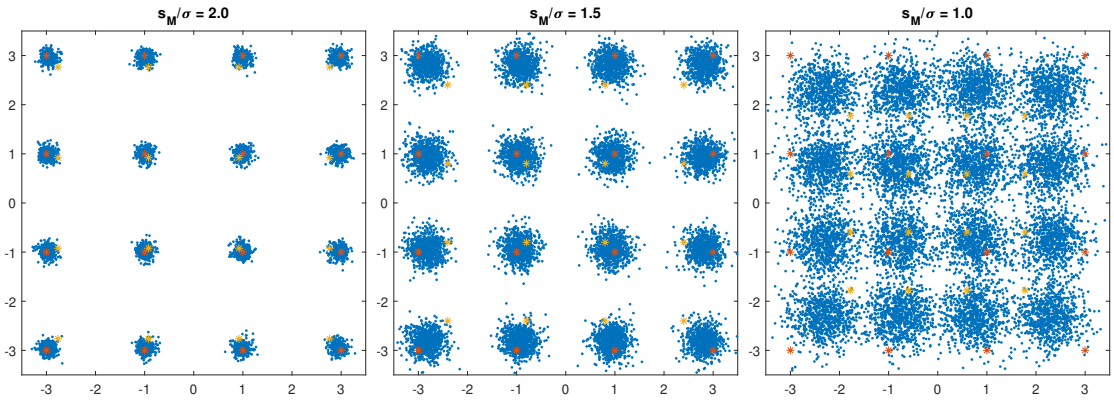

Figure 3.4: I-Q plot of 100 symbols after an SEL operation considering different clipping thresholds and OFDM with $N = 128$ subcarriers and 16-QAM constellations. The original constellation points are marked in orange and their linear Bussgang counterpart are represented in yellow.

Figure 3.5 presents the normalized instantaneous power of one of the OFDM symbols of figure 3.4 subjected to the same three nonlinear operations. It allows having an insight into the resulting nonlinearly distorted signal (i.e., an idea of the scale of the saturation). Notice that while the threshold s_M/σ is an amplitude and not power, the figure's vertical axis corresponds to power values.

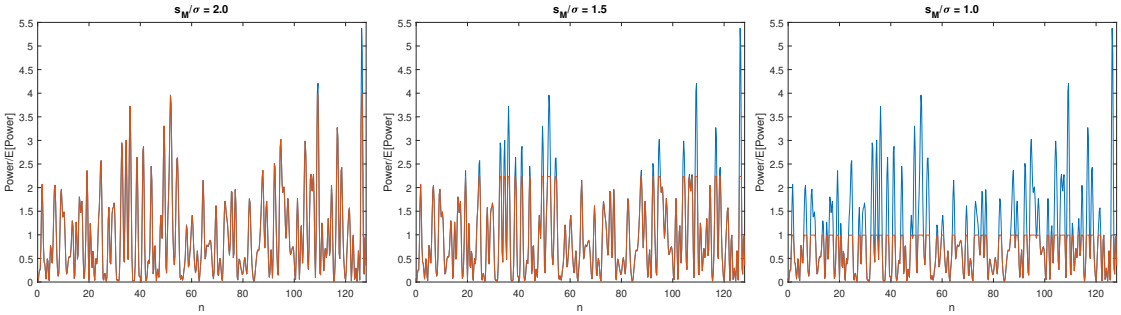

Figure 3.5: Normalized power of input OFDM signal after an SEL operation with different thresholds considering 16-QAM constellations and 128 subcarriers.

3.3 Drawbacks

An important disadvantage of OFDM is the large envelope fluctuations of the signal which is associated with its multicarrier nature (i.e., the summation of different carriers with different amplitudes and phases). The sporadically large peaks greatly impact the energy efficiency of the system's PA, which has to be designed to keep the high power peaks of the signal in its linear region, thus making it overpowered for the majority of the time. This therefore substantially reduces the amplification efficiency.

Figure 3.6 shows the instantaneous normalized power of an OFDM symbol with $N = 128$ subcarriers and 16-QAM constellations. It can be observed that for this randomly

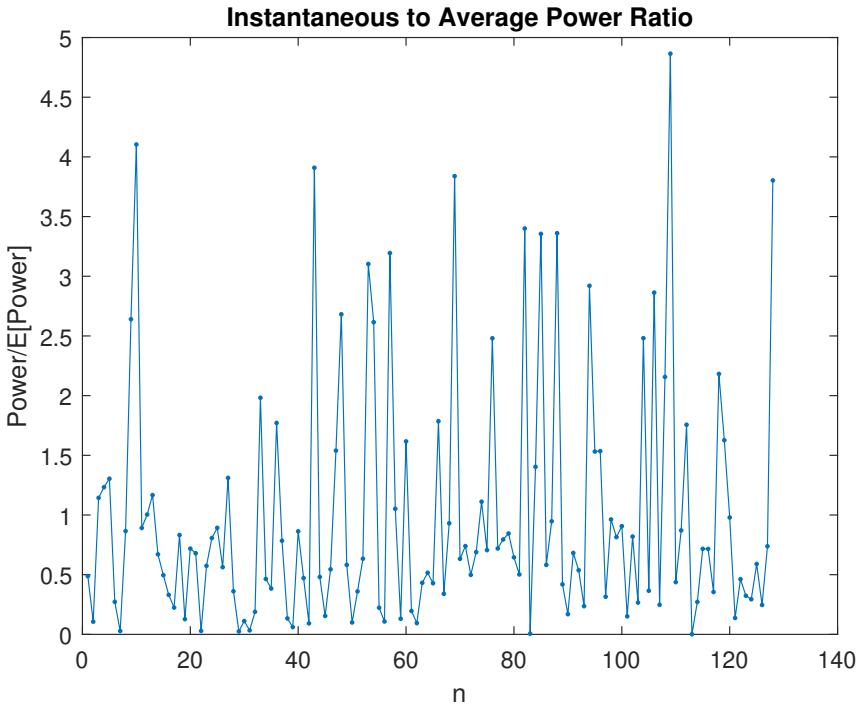

Figure 3.6: Instantaneous to average power ratio of an OFDM signal with $N = 128$ subcarriers and 16-QAM constellations.

generated OFDM signal, the peak power is almost 5 times larger than the average power (i.e., these powers have approximately a 7 dB difference). Many other peaks are observed but for most of the symbol duration, the peak power is below 1.5 times the average power (about 1.8 dB).

In fact, it can be shown by the central limit theorem that for a sufficiently large number of subcarriers, the real and imaginary part of an OFDM symbol in the time domain follow a Gaussian distribution, so that large power peaks occur with nonzero probability [23]. As a consequence, the magnitude of the OFDM signals follows a Rayleigh distribution. The Gaussian nature of OFDM signals can be observed in figure 3.7, where the PDFs of the real part, imaginary part, and absolute value of an OFDM signal with $N = 128$ subcarriers and 16-QAM are shown.

Clearly, even with a moderate number of subcarriers (in this case $N = 128$), the simulated PDF of the real and imaginary parts are well modeled by a Gaussian distribution.

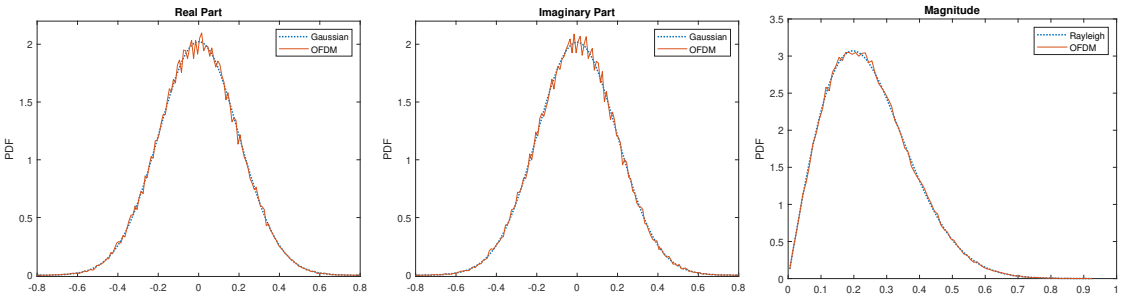

Figure 3.7: PDFs of the real part, imaginary part and absolute value of an OFDM signal with $N = 128$ subcarriers and 16-QAM symbols.

From the figure it can be observed that the Gaussian approximation for modeling the PDF of OFDM signals is accurate, even with a moderate number of subcarriers.

3.3.1 Super-QAM Constellations

The ever-present demand for higher data rates in wireless communications requires the continuous development of new techniques and/or improvement of current ones.

In OFDM systems there are three main ways to improve the data throughput, namely: (i) increasing the symbol frequency, (ii) increasing the number of subcarriers and (iii) increasing the size of constellation employed on each subcarrier. All three are effective but also limited by wireless channel characteristics, bandwidth restrictions and/or technology improvements.

Higher frequency symbols are achieved by decreasing the pulse function period, but due to ISI its effectiveness is bounded by the size of the guard interval between symbols that is dependent on the wireless channel's intrinsic multipath time delays.

Increasing the number of data streams comes with the price of a larger bandwidth which in the current already highly populated wireless RF spectrum, is undesirable.

Larger constellation sizes come as the natural way to keep improving OFDM's data rates. The constraint in the constellation size case is that the linearity requirement of the PA becomes even more stringent with a larger constellation's size. To illustrate this effect it is shown in figure 3.8 the complex amplitude plot of several OFDM signals with different constellations impaired by the same clipping level s_M/σ.

From the figure, it can be observed that a relatively high saturation level for a 16-QAM signal can become severe when employing 256-QAM even though it seems that the time domain signal and OOB emissions might look similar to the ones of a smaller constellation.

In fact, the in-band degradation caused by saturation of the signal becomes an exorbitant issue at super QAM constellations, where constellations can have $M = 1024$ (32×32) points or more. To make the BER acceptable for larger constellations, techniques that

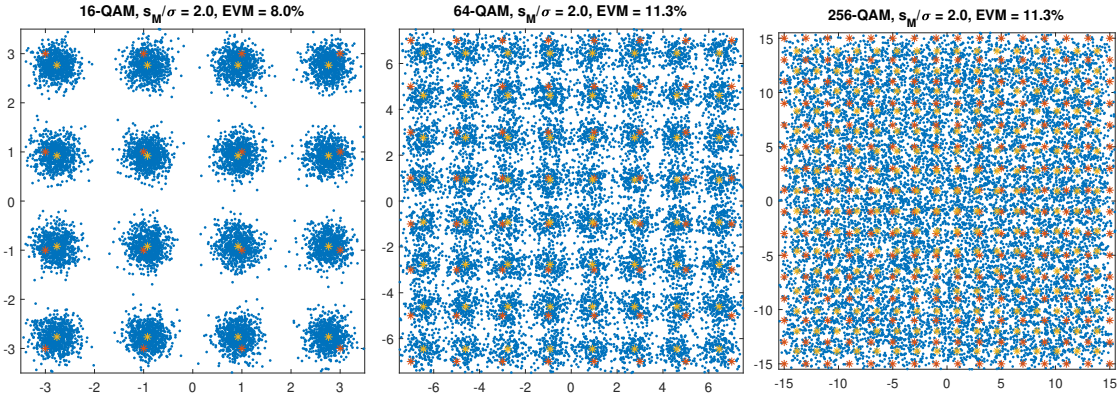

Figure 3.8: Effect of nonlinearity of constellation spread for different constellation sizes.

introduce additional complexity to the receiver, such as the ones presented in chapter 2 are necessary to mitigate these effects.

3.4 Metrics

The magnitude of an OFDM signal follows a Rayleigh distribution which means that high power peaks in a symbol can take place with a non-zero probability. The high power peaks in the signal make OFDM susceptible to nonlinear distortion effects, especially the ones resulting from amplitude saturation at the PA stage.

Let us define PAPR, which is a metric for quantifying the scale of the OFDM symbol's envelope fluctuations in relation to the average power. PAPR is defined by the ratio between the maximum power and the average power of a given OFDM symbol, and is expressed in decibels as

$$PAPR = 10log_{10}\left(\frac{\max(|s_n|^2)}{E[|s_n|^2]}\right), \tag{3.19}$$

where $max(|s_n|^2)$ is the peak-power and $E[|s_n|^2]$ represents the average power of a given OFDM symbol.

Figure 3.9 presents both the PAPR and the BER of a conventional receiver considering 16-QAM OFDM system impaired by SEL with different saturation levels s_M/σ. The signal is not encoded or has any channel effect, i.e. the receiver has the exact same signal from the transmitter, and the data estimates are obtained by a hard decision decoder. Taking into account that the channel noise will further increase the BER, it can be observed from the figure that for high saturation levels the distortion effect is somewhat negligible, but for saturation levels $S_M/\sigma < 2.0$ the system will experience severe degradation.

It is important to note that each OFDM symbol has its own PAPR value and not all symbols have high PAPR. Therefore, the PAPR can be seen as a random quantity and can be studied statistically [24]. As a consequence, is only possible to know the probability that a symbol has a PAPR larger than an arbitrary value [25]. This probability is presented in a CCDF plot that gives a better perspective on a technique's effectiveness to reduce the

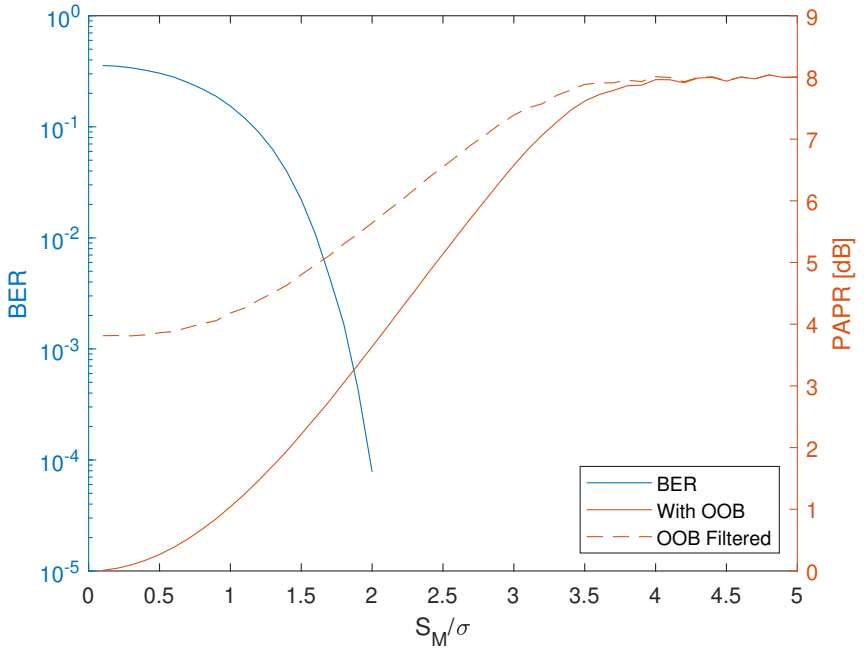

Figure 3.9: SEL effect PAPR and BER. 16-QAM, 128 subcarrier, with and without OOB noise filtered, averaged for 1000 symbols. BER is computed using a hard decision decoder directly from the output of the distortion operation. BER is the plot on the left, PAPR are the plots on the right

PAPR. CCDF can be simply expressed by

$$CCDF(x) = p(PAPR > x). \tag{3.20}$$

The CCDF is usually shown in a logarithmic plot where the Y-axis is the probability of a symbol having a PAPR larger than X and the X-axis is the PAPR in decibels.

The CCDF can give an insight into the effectiveness of the different techniques to reduce PAPR of an OFDM signal. A simple and efficient way to reduce the PAPR is to deliberately clip the OFDM signal considering a given clipping level s_M, operation described by SEL. An example of a CCDF plot is shown in figure 3.10.

Naturally, a desirable CCDF is a curve with its area closest as possible to a PAPR of 0 dB, which translates to the possibility of high power peaks being almost nonexistent. In the figure, it can be observed that even when a relatively high clipping level of $s_M/\sigma = 2.0$ is employed, the signal's PAPR can be considerably reduced. This comes at a cost of introduced nonlinear distortion, which not only leads to performance degradation due to the in-band component of the distortion but also to spectral growth, with the so-called OOB emissions. These emissions can be mitigated with a filtering operation. However, as can be observed in figure 3.10, the filtering operation leads to regrowth and higher PAPR.

In order to manage this PAPR regrowth, an iterative clipping and filtering process may be employed [26]. This comes with the cost of high complexity: for a process of K iterations, $2K + 1$ Fourier transform operations are necessary. However, the in-band distortion is not so easy to remove. In a typical OFDM signal with nonlinear distortion,

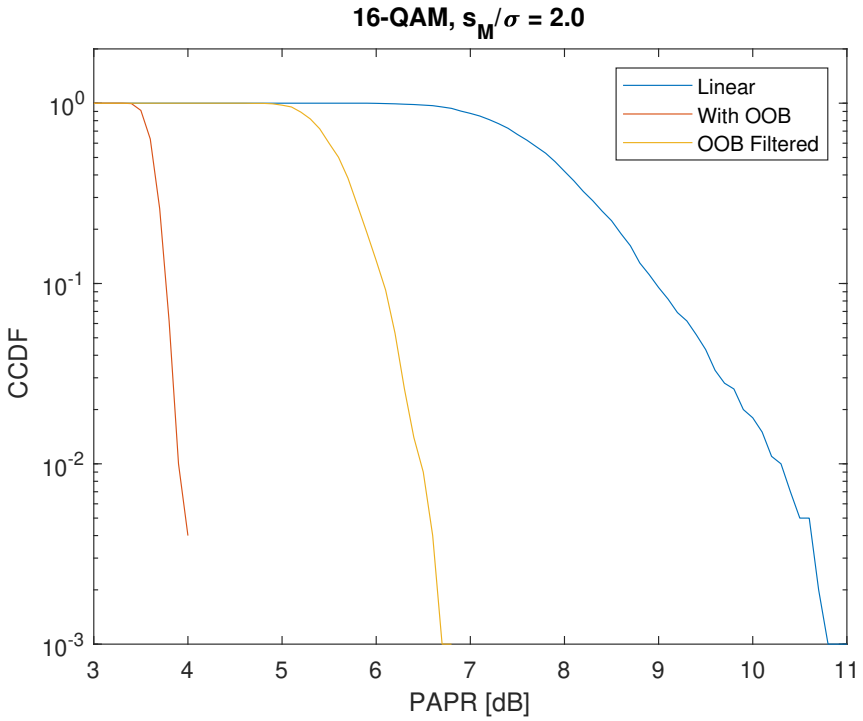

Figure 3.10: CCDF of the PAPR considering OFDM signals with $N = 128$ subcarriers and 16-QAM. The clipped OFDM signals have a clipping level of $s_M = 2.0$.

a CCDF curve with a noticeable probability at high power correlates with a high BER, although BER cannot be evaluated from the CCDF alone [23].

Besides the clipping technique for reducing PAPR, other techniques can be encountered in the literature, such as the distortionless PAPR-reducing techniques [11, 23]. These methods can be employed to avoid excessively high power peaks while keeping the system linear. They generally operate by generating a set of different OFDM symbols for the same bit sequence and transmit the one with the lowest power peaks. To this extent it's assumed that by modifying the originating bit sequence a symbol with more desirable characteristics can be obtained. Below are presented three of these methods:

- Interleaving method – Interleave signal with known bit sequences.
- Selective mapping - Modulation of the source bits with various constellation mapping schemes, i.e. by redefining what sequence of data bits corresponds to which point of the constellation [11, 23].
- Adjusting the constellation - Modulation of the source bits with different sizes and types of constellations [11, 23].

These techniques decrease the peak power of the signal but have drawbacks. First, bits of side information needs to be transmitted along with the original bit sequence, increasing the size of the symbols, and if that information is corrupted then all the symbol's data is lost. Second, additional complexity on the transmitter is needed to perform a Fourier

transform operation for every candidate symbol. Third, the effectiveness in decreasing power peaks is very limited, as it can be seen in figure 3.10 where is shown that in the case of a 16-QAM linear symbol it is almost certain that the peak to average power will never be lower than 7 dB, independently of the bit sequence.

In conclusion, it is very difficult to have both a low PAPR to increase amplification efficiency and also maintain the signal linearity. Therefore, nonlinear distortion effects in OFDM are generally unavoidable. Not being able to mitigate nonlinear effects before the transmission, then one option is to mitigate them at the receiver.

EVM is a widely used metric to measure the degradation of digitally modulated signals [27, 28]. It specifies the deviation between the ideal position and the measured position of the constellation of a signal. In the case of OFDM, the signal's EVM can be used to measure the dispersion of points in the constellation caused by nonlinear distortion and is an essential factor for specifying the performance [2]. EVM is defined as the ratio of the root mean square (RMS) power of the error vector to the RMS power of the reference signal constellation, which can be expressed as

$$EVM = \sqrt{\frac{\sum_{k=0}^{N-1} |X_k - R_k|^2}{\sum_{k=0}^{N-1} |R_k|^2}} \times 100\%, \tag{3.21}$$

where R_k is a reference signal (i.e., the undistorted constellation point before the nonlinearity) and X_k is the distorted signal. To compute the correct EVM when modeling an OFDM system, the linear coefficient α between the original and the distorted signal has to be accounted for.

As presented in figure 3.11, EVM condenses the phase and amplitude error of a signal in a single value. The larger the EVM value is, the wider the dispersion from the ideal constellation and, consequently, the larger the signal degradation.

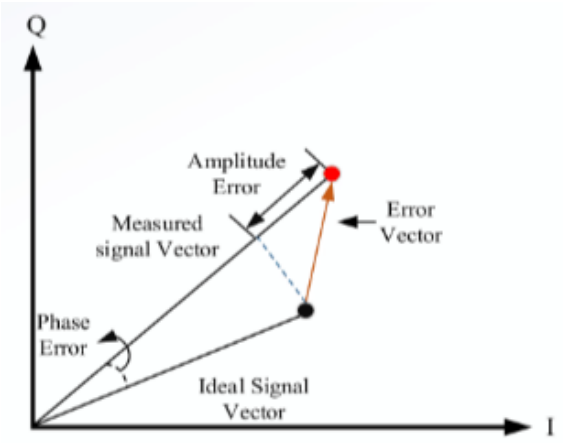

Figure 3.11: Geometry associated to the computation of EVM [2].

In addition to the distortion of the constellation caused by the in-band distortion, the saturation of an OFDM signal also results in a phenomenon called spectral broadening that leads to OOB emissions that might interfere with adjacent bands. Figure 3.12 shows a nonlinear OFDM symbol in frequency and time domains. The OOB component is evident even though most of the time domain signal stays intact after the nonlinear operation. The tendency of OOB emissions is to aggravate for lower saturation thresholds.

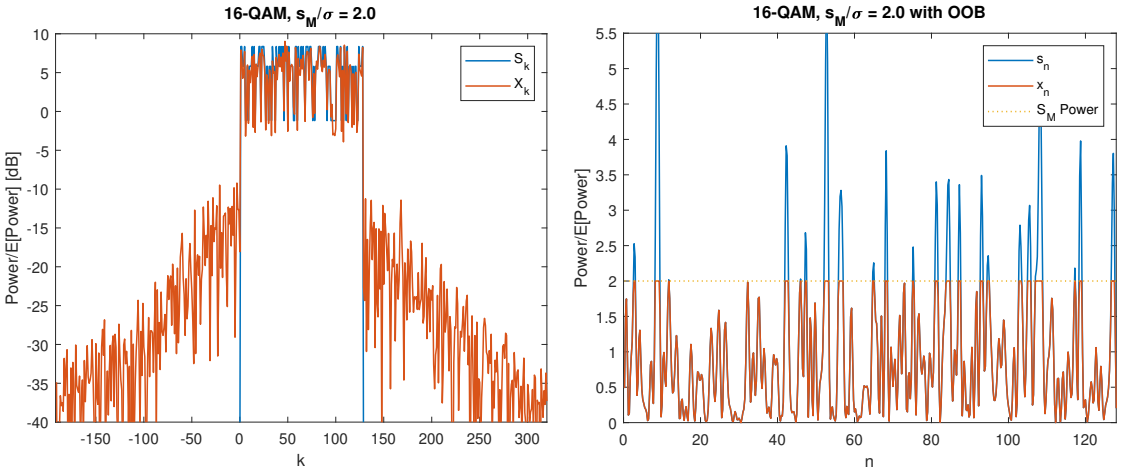

Figure 3.12: Evolution of the frequency-domain (left figure) and time-domain (right figure) OFDM signal with 16-QAM constellation and $N = 128$ subcarriers with OOB component.

This OOB undesirable effect can be suppressed by lowpass filtering but as a consequence, the peak power of the resulting signal increases [9, 23], as can be observed in figure 3.13 where for that OFDM symbol the peak to average power has a growth of 1.5 when compared to the signal before filtering, as can be observed in figure 3.12.

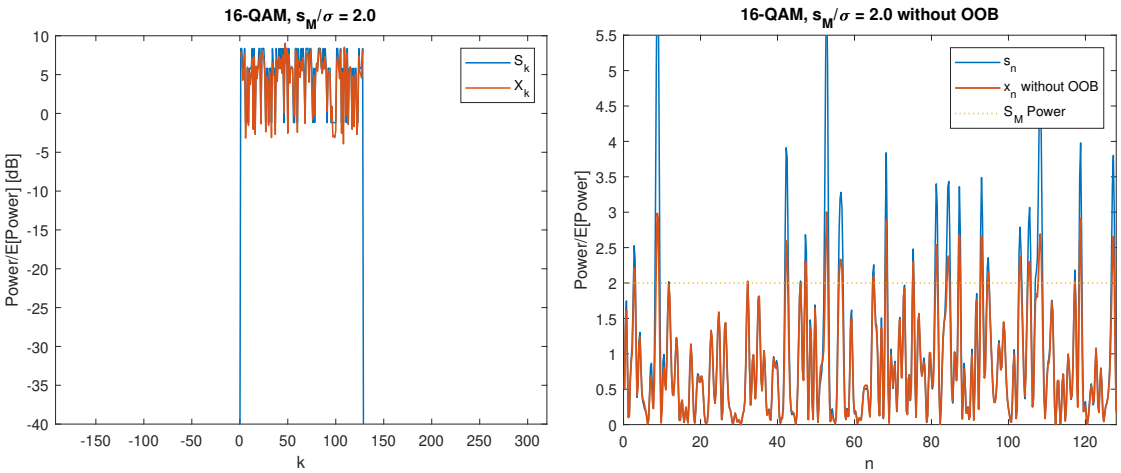

Figure 3.13: Evolution of the frequency-domain (left figure) and time-domain (right figure) OFDM signal with 16-QAM constellation and $N = 128$ subcarriers with OOB component filtered out.

In this chapter it was shown that due to its intrinsic high PAPR, nonlinear distortion is almost unavoidable in OFDM signals and should be accounted for when designing OFDM schemes. This undesirable nonlinear distortion usually occurs at the transmitter's PA,

when the high peaks of the signal force it to work outside its linear region or by deliberate clipping of the signal and can be modeled as described in section 3.2.1. By having at the receiver end of the system both the distorted signal and the model of the nonlinearity that exists in the transmitter, a better estimation of the original signal can be achieved, as concluded in section 2.2.1 where the BNC algorithm is presented.

4

Design of Practical Bussgang Receivers

In this chapter, Bussgang receivers will be studied in more detail. This type of receiver is based on the Bussgang theorem which splits a saturated signal into two components: a linear and an uncorrelated distortion component, as seen in section 3.2.2. Through multiple iterations BNC, algorithms estimate the distortion component and removes it from the received signal, resulting in a better estimation of the original signal than if using a simple hard decision demodulator. This last statement will be tested against a wide range of parameters of saturation models. Moreover, since in practical systems, the nonlinearity that exists at the transmitter is not perfectly known at the receiver, this chapter presents algorithms to estimate the nonlinearity model. The estimation performance of these algorithms is analyzed and the performance of Bussgang receivers with estimated nonlinearities is investigated.

This chapter is organized as follows: in section 4.1 is studied the improvement of BER of BNC receivers over conventional receivers. A model of the distortion is needed for the BNC receiver to function, thus in section 4.2 two algorithms for estimation of PA model are presented. In section 4.3 the performance of BNC receivers with estimated distortion models is analyzed.

4.1 Limitations of Bussgang Receiver

An OFDM system with a traditional receiver is depicted by the block diagram in figure 4.1. The nonlinear distortion introduced in the transmitter by the power amplifier is included.

This receiver is designed with the assumption that the signal after equalization is composed by the transmitted OFDM symbols and a normal distributed noise added by the wireless channel. This additional noise is expected to have no correlation with the desired transmitted signal and be unpredictable. The receiver extracts the estimation of the transmitted signal from the noisy signal by means of hard decision demodulator and thus if the transmitted signal overpowers the channel noise then the receiver can make accurate estimations (if given perfect equalization).

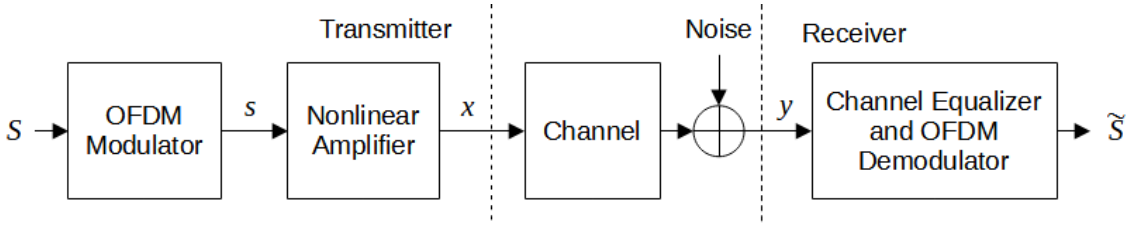

Figure 4.1: Block diagram of a system with nonlinear distortion and a traditional receiver.

The block diagram can be expressed analytically by the equations

$$x = f(IFFT(S)) = \alpha s + d \tag{4.1}$$

$$y = h * x + n \tag{4.2}$$

$$\tilde{S} = HardDecision(H^{-1}Y), \tag{4.3}$$

where lower-case letters represent signal in time domain and upper-case in frquency domain.

As shown in equation (4.1), the received signal has one more component due to the effect of the nonlinear amplifier: the distortion component. The decomposition of the distorted signal into two components is stated by the Bussgang theorem and introduced in section 3.2.2. In this scenario, the traditional receiver assumes the distortion component of the signal as part of the channel's noise.

Consequences in terms of BER performance of that assumption can be observed in figure 4.2, which presents the effect of SEL PA on the BER plot of a 16-QAM, 128 subcarrier system with a traditional receiver. Each BER curve corresponds to a different saturation level of the SEL model.

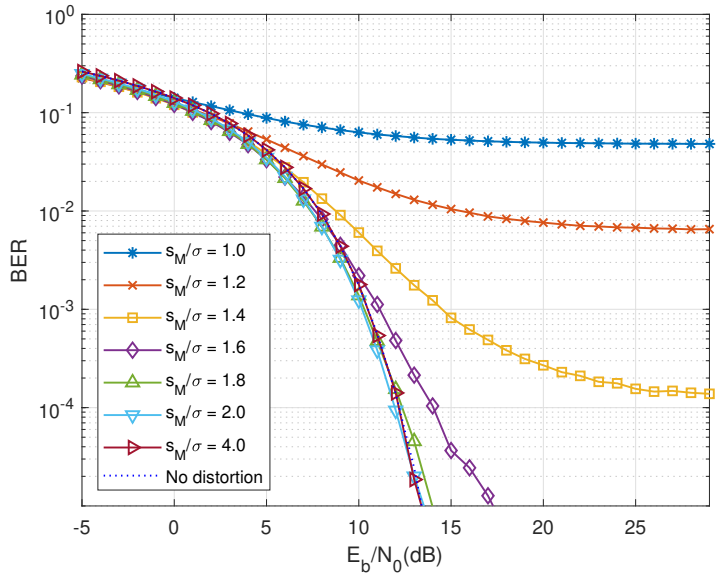

Figure 4.2: Impact of a SEL amplifier on BER.

As can be observed from the figure, the harshest saturation $s_M = 1.0$ corresponds to

the worst BER, since in this scenario the nonlinear distortion effects are stronger. As expected, by increasing s_M the BER gets progressively better. The plots follow the BER of a linear power amplifier, plotted as the dotted line, until certain point where it diverges and eventually settles at an apparent asymptote. This result is supported by Bussgang's theorem which shows that the distortion component power increases linearly with the linear component and eventually overpowers the noise of the channel, resulting in a SNR equal to the linear component power over the distortion component power. For the rest of this document that asymptote is named BER floor.

It is concluded that increasing the power of the transmission in order to obtain a higher SNR has limited gains when the OFDM signal suffers from nonlinear distortion, especially for stronger distortion levels.

One interesting experiment is to see what happens when the nonlinear distortion component is perfectly known on the receiver side. This scenario is depicted in figure 4.3, which is an extension of figure 4.1.

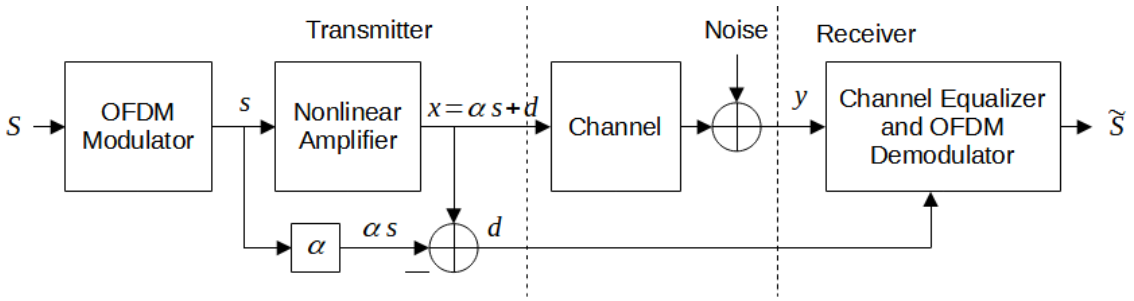

Figure 4.3: Block diagram of a system with the exact distortion component available at the receiver.

As can be noted, this modified receiver simply subtracts the distortion component from the received signal. This system can be expressed by the equations

$$x = f(IFFT(S)) \tag{4.4}$$

$$y = h * x + n \tag{4.5}$$

$$d = x - \alpha s \tag{4.6}$$

$$\tilde{S} = HardDecision(H^{-1}Y - FFT(d)). \tag{4.7}$$

The benefit of having distortion information at the receiver is observed in figure 4.4, where it is shown the BER considering the same nonlinear OFDM transmissions of 4.2.

From the figure, it can be noted that the achievable BER in these conditions is very close to the linear OFDM performance. This is to be expected since channel equalization allows for the signal to pass undisturbed, and by subtracting the distortion component and dividing by alpha the linear signal plus channel noise is obtained just like in a traditional OFDM system.

Unfortunately, sending the intact distortion component of the signal in parallel with the wireless channel is not feasible in pratical implementation. To achieve the same gains in

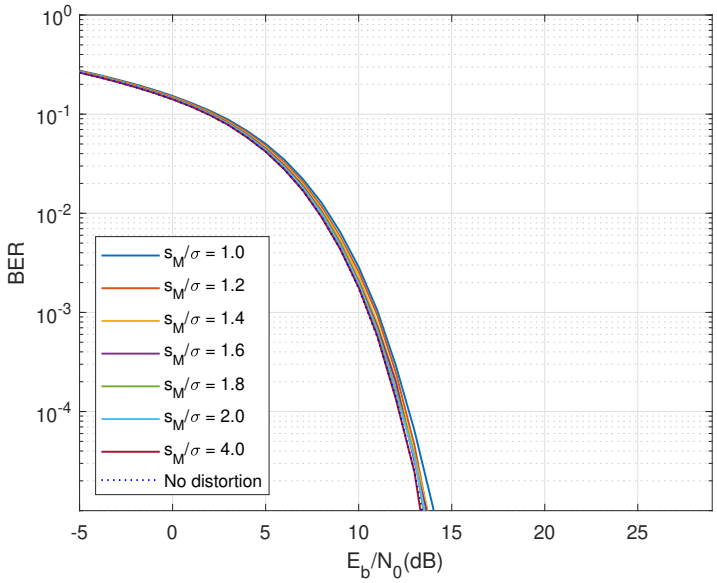

Figure 4.4: Effect of different saturation values on the BER of a nonlinear OFDM system if the receiver has the exact distortion component.

a real implementation of an OFDM system the distortion component has to be estimated from the received signal, and this is precisely what is done in Bussgang receivers. Figure 4.5 presents a block diagram of an OFDM system that at the receiver can accurately reproduce the distortion effects caused by the nonlinear PA.

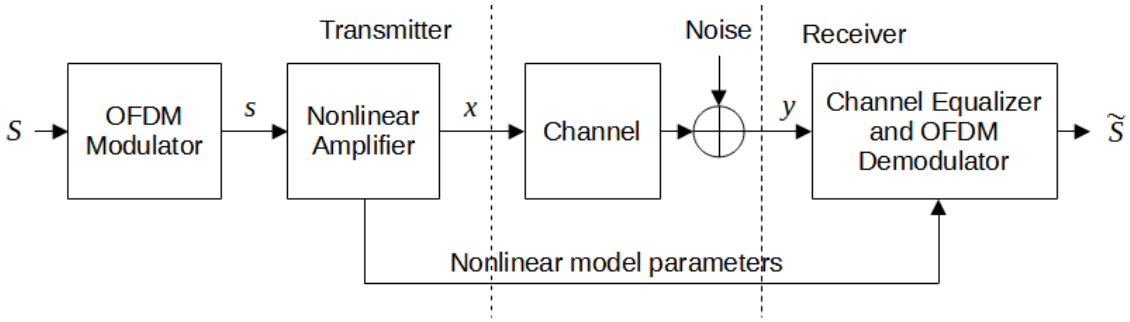

Figure 4.5: Block diagram of a system where the model parameters of the nonlinear amplifier are known at the receiver.

It should be noted that in contrast to the receiver in figure 4.3, this receiver has no information about the distorted signal other than the PA model parameters. A BNC algorithm is present at the receiver to make better estimations of the signal before distortion with the aid of the nonlinear parameters. As mentioned before, since the estimation of the distortion is made with the aid of Bussgang's theorem, this type of receiver is named Bussgang receiver.

Figure 4.6 shows the block diagram of a BNC algorithm. In the figure, $Y_I[0]$ is the received OFDM symbol after equalization and $Y_I[n]$ is the estimation of the symbol before distortion at the transmitter. The estimation is iterative and the first value of Y_I is the

equalized symbol. $Y_I[n]$ is demodulated and again modulated into symbol B as this is the estimated transmitted linear signal at the n^{th} iteration. Then, the same nonlinear operation of the transmitter is applied to B_k and followed by the removal of the linear component of Bussgang's theorem, resulting in the estimated distortion at the n^{th} iteration. This estimated distortion is then removed from the received symbol $Y_I[0]$ and the symbol of the next iteration $Y_I[n+1]$ is computed. The final Y_I is then passed along to the traditional hard decision demodulator, which is not depicted in the figure, where assumed channel noise is removed.

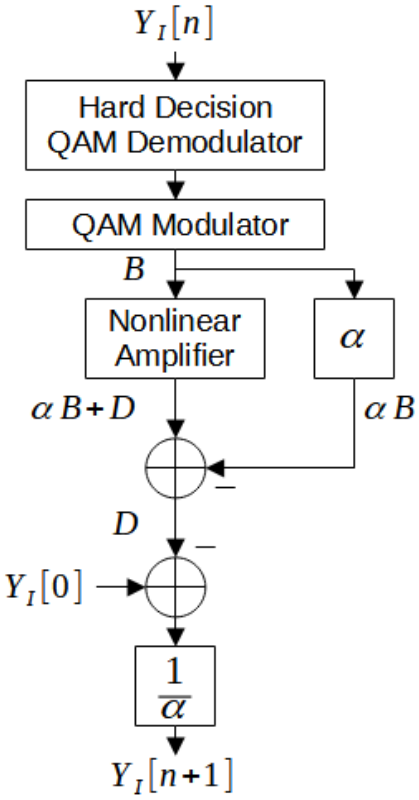

Figure 4.6: Block diagram of a BNC algorithm.

An alternative version of the BNC algorithm with a better BER performance, according to the simulations done, is presented in figure 4.7 where the Bussgang's α factor is not present.

In this version, the estimation distortion is not just the distortion component of the Bussgang theorem, D, but also part of the linear component, as D'. Given that D is in fact correlated with the linear signal S, then is not surprising that the receiver keeps on working correctly with the additional linear component in the distortion estimation. The reshaping of the Bussgang theorem equation is as follows.

$$X = \alpha S + D = S + (D + (\alpha - 1)S) = S + D'. \tag{4.8}$$

The better performance of the alternative BNC algorithm can be explained by the absence of the α factor. α is a number intrinsic of the nonlinear model and thus it is a

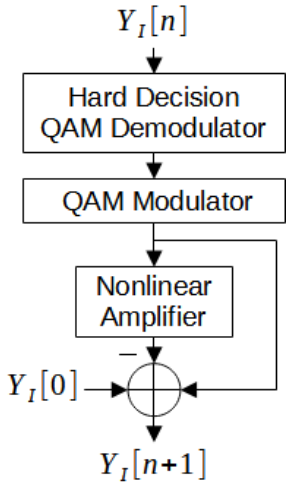

Figure 4.7: Block diagram of the alternative BNC algorithm.

function of the nonlinear model parameters and computed as the average α value of all possible OFDM symbols, as defined by equation (3.16). The consequence is a mismatch between the average α and the actual α of the symbol, and the resulting worse BER. By removing the explicit α factor from the BNC algorithm the mismatch is avoided.

The BER of a nonlinear OFDM system with BNC receiver is shown in figure 4.8. These results can be compared with the ones of figure 4.2 and confirm the great benefit that knowing the distortion model parameters at the receiver can bring to the performance of a nonlinear OFDM system when compared with a conventional receiver. Note that the BER floor for the stronger saturation level of $s_M/\sigma = 1.0$ is substantially lower. More concretely, it is less than one percent of the BER floor of the traditional receiver. Moreover, for higher saturation levels, is observed just a slight divergence in the performance of a system with no nonlinear distortion.

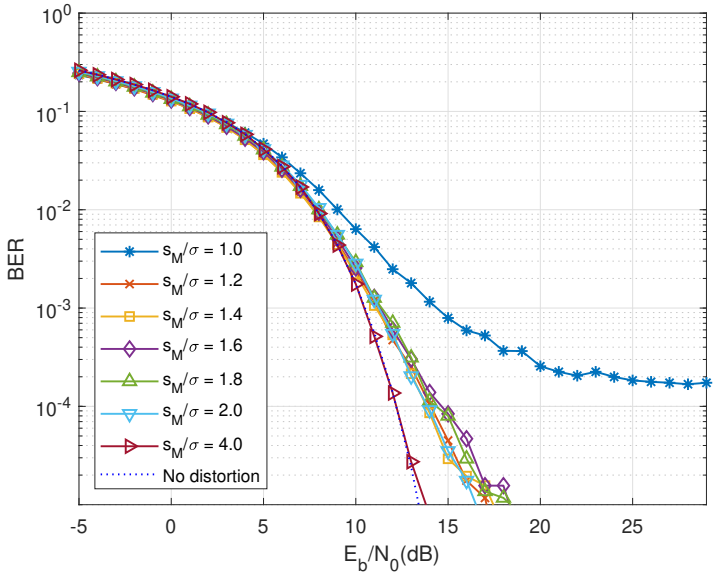

Figure 4.8: Effect of different saturation values on BER with a BNC receiver of 10 iterations.

It is clear that a BNC receiver greatly improves the BER curve on systems with nonlinear distortion, but one downside of the implementation is the increased complexity. In order to minimize the complexity of the algorithm the BER plots of each iteration of the BNC receiver considering a nonlinear distortion of $s_M/\sigma = 1.2$ are presented in figure 4.9. From the figure, it can be noted that the first iteration of the BNC algorithm has a great effect on lowering BER. The second iteration also brings improvements but any iteration after does not give a noticeable gain. Therefore, it can be concluded that two iterations are enough for the BNC algorithm to converge to the best BER it can achieve.

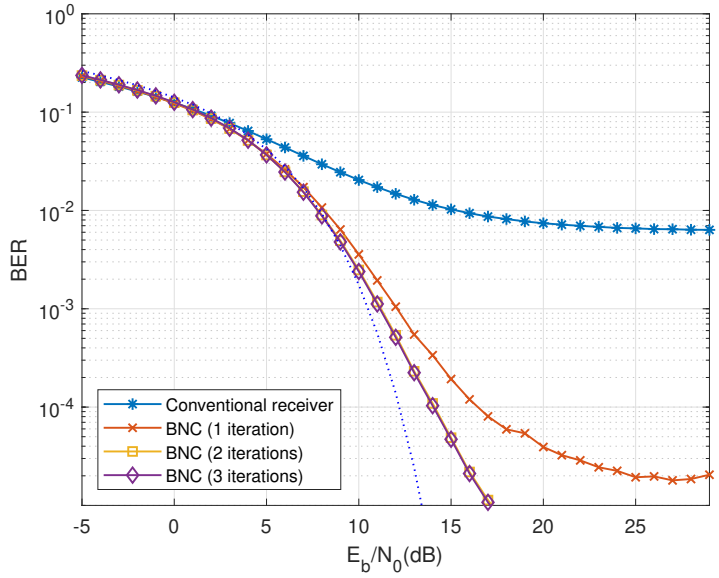

Figure 4.9: Effect of the number of iterations of the BNC receiver on the BER for $s_M/\sigma = 1.2$.

As a final comparison between a traditional and a BNC receiver, figure 4.10 demonstrates the BER floor as a function of saturation level s_M/σ, for a SEL distortion. From the figure, the benefits of a BNC receiver can be clearly observed. As clipping levels larger than $s_M/\sigma = 0.3$, the BER floor is better than the conventional receiver. For instance, at $s_M/\sigma = 1.2$ it is more than a thousand times lower than the BER of conventional receivers. It should be also noted that the plot for BNC receiver ends at $s_M/\sigma = 1.2$, which is an extremely strong nonlinear distortion level. For higher values of s_M/σ, it can be extrapolated that the BNC curve will continue to be much better than the traditional receiver until the point where the saturation level is so high that it has no effect on the signal and both curves will be equal.

4.2 Algorithms for Estimation of Nonlinearity Parameters

As seen above for OFDM systems with nonlinear distortion, a system of the type seen in figure 4.3, where the distortion component of the signal is completely known at the receiver would be great but would also require a parallel and ideal channel, which other than being impractical in a real scenario, completely misconstrue the wireless communication

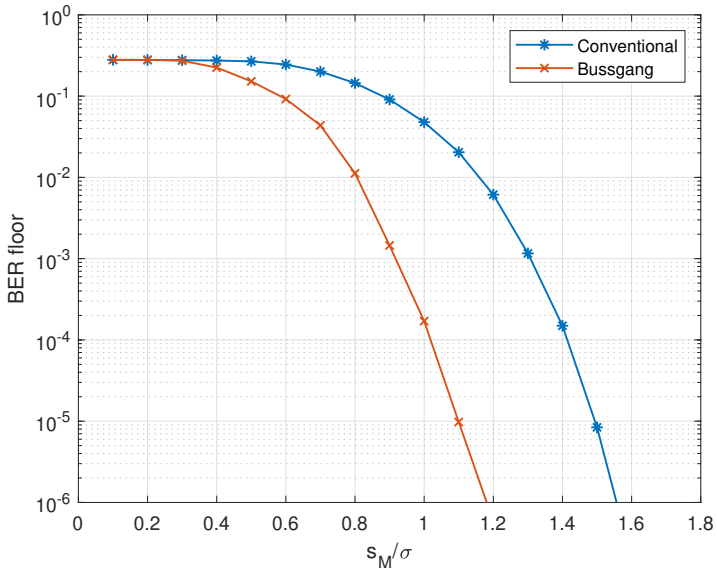

Figure 4.10: Comparison of BER floor in function of saturation level s_M/σ.

challenge. The solution found was to employ a BNC receiver that estimates the distortion component by knowing a model of the transmitter's power amplifier, as described in section 3.2.1. This model is specified by its parameters which in figure 3.4 depicts as being sent from the transmitter to the receiver in an ideal parallel channel, but unlike the previous system, this parallel information can be estimated from the received signal, as will be shown in this section.

To keep consistency with the previous section the figure 4.11 is shown, where the receiver estimates the nonlinear amplifier model's parameters from the received signal. These estimated parameters are used by the BNC algorithm and it is expected that inaccuracies of the parameters result in an OFDM system of low performance. In extreme cases, incorrect parameter estimation can lead to a receiver with poorer performance than a conventional one.

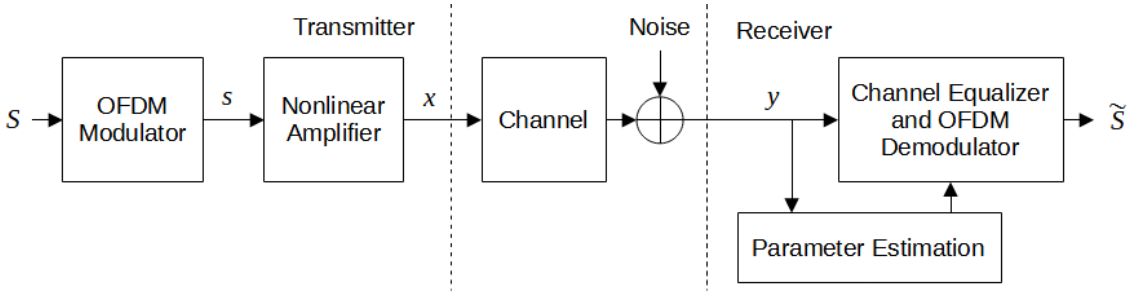

Figure 4.11: Block diagram of a system where the model parameters from the nonlinear amplifier are estimated from the received signal.

By estimating the model of the distortion instead of using fixed parameters, the receiver has the flexibility to adapt on the fly to physical changes on the transmitter's power amplifier due to temperature or any other phenomenon.

4.2.1 PDF-Based Estimation

Given that the models used to describe the nonlinear distortion of the transmitter's power amplifier introduced in section 3.2.1, mostly affect the instantaneous magnitude of the signal then is feasible to obtain a characteristic curve of that model on the PDF of the distorted signal's instantaneous magnitude. One advantage of this method is that it can be applied to any received signal, thus there is no need for transmissions of pilot symbols (i.e., large overheads).

An OFDM signal is characterized in its PDF of instantaneous magnitude as a Rayleigh distribution (see figure 3.7). Under these conditions, by analyzing the density migration of PDF from the original to the distorted signal, parameters of the distortion model such as the saturation level can be estimated. Figure 4.12 shows the effect of SEL distortion in the PDF of the magnitude of a nonlinearly distorted OFDM signal considering different saturation levels.

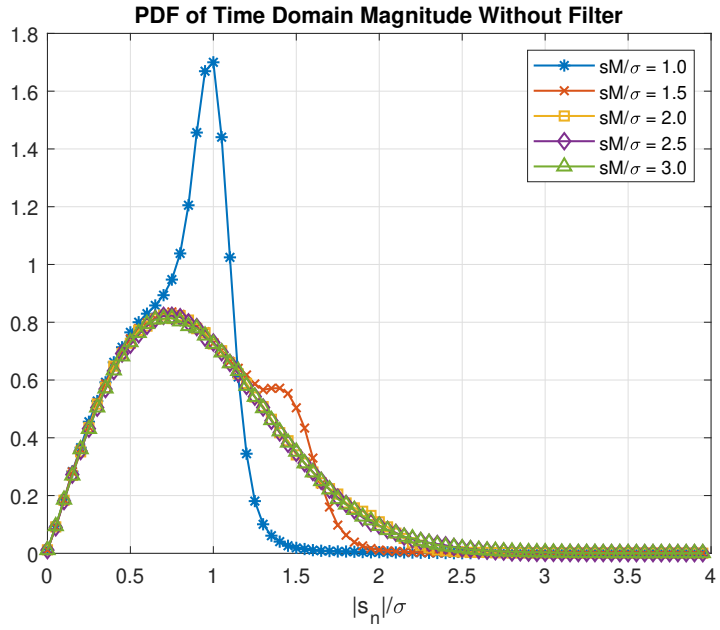

Figure 4.12: PDF of received signal magnitude for multiple saturation levels.

From the figure, it can be noted that all plots follow a Rayleigh-like distribution while below the saturation threshold. At that point, a peak emerges and afterward, the probability quickly falls to zero. It can be observed that the area of the tail of the Rayleigh distribution migrates to the peak. Thus, for lower saturation levels the estimation of s_M/σ can be made accurately by simply selecting the point of higher probability. For larger values of s_M/σ, the threshold peak loses prominence which makes the estimation difficult and less precise.

A downside of this method is that the channel noise also affects the PDF. Figure 4.13 shows the PDF of a nonlinearly distorted OFDM signal considering $s_M/\sigma = 1.0$ and different values of SNR.

It can be seen from the figure that for $SNR > 5dB$ this method of estimating the

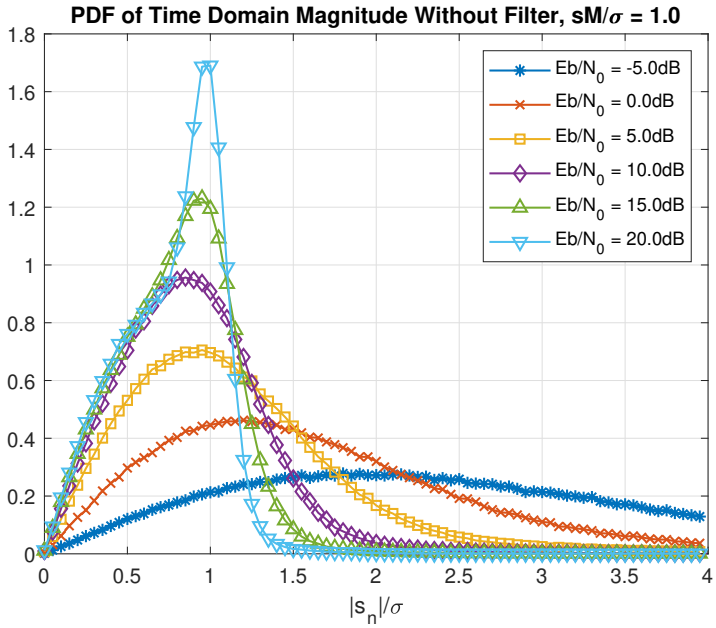

Figure 4.13: PDF of received signal magnitude considering different values of SNR.

saturation level by selecting the point of maximum probability is viable. However, lower values of SNR considerably affect the performance of this estimation method.

In conclusion, the PDF-based method for estimating the nonlinearity parameters is limited, being only viable for estimating the saturation level s_M/σ when nonlinear distortion effects are strong. For this reason, another estimation method investigated in this thesis for the parameters of the nonlinear model is the curve fitting method.

4.2.2 Least Squares Curve Fitting and Frame Design

The curve fitting method principle is explained in the following: The transmitter and receiver arrange a special transmission of a symbol s that is already known by the receiver. The receiver by having both s and the received y, which is a distortion of s done by the transmitter's power amplifier and contains noise from the channel, can estimate a distortion model $\tilde{f}$ that turns s into y. This is accomplished by testing many models of the distortion in a convergence process and minimizing the error $y - \tilde{f}(s)$, resulting in a curve that best fits the magnitude of the received signal.

This estimation method requires the transmission of pilot symbols, which are known by both the transmitter and receiver, but has the advantage of being able to estimate distortion model parameters other than just the saturation level s_M/σ of a SEL PA, unlike the PDF method, and as we'll see it can give precise estimations.

For the remainder of this section, the least squares algorithm is chosen as the optimization function of the curve fitting method because of its simplicity. The least squares

curve fitting estimation algorithm can be formulated in the following formula

$$\underset{\tilde{f}}{\operatorname{argmin}} \left\{ \sum_{n=0}^{N-1} |\tilde{f}(s_n) - y_n|^2 \right\}, \tag{4.9}$$

where $\tilde{f}(\cdot)$ is the estimated nonlinear function. This function can be described by a nonlinear distortion model with its parameters defined in the parameter vector $\boldsymbol{\theta}$ and can be solved with the aid of a gradient descent algorithm [29]. This is expressed as follows

$$\underset{\boldsymbol{\theta}}{\operatorname{argmin}} \left\{ \sum_{n=0}^{N-1} |f(s_n, \boldsymbol{\theta}) - y_n|^2 \right\}, \tag{4.10}$$

and the gradient descent algorithm that computes the arguments for the minimum is given by k iterations of the procedure

$$\theta_i^{k+1} = \theta_i^k - \mu_i \frac{\partial g(\boldsymbol{\theta})}{\partial \theta_i}|_{\boldsymbol{\theta}^k}, \tag{4.11}$$

where μ_i is the step size of the i^{th} variable in vector $\boldsymbol{\theta}$ and $g = \sum_{n=0}^{N-1} |\tilde{f}(s_n) - y_n|^2$, $\boldsymbol{\theta}$ converges to a local minimum of g. The smaller the values of vector $\boldsymbol{\mu}$, the more accurate the algorithm is but more iterations are needed. Therefore, this algorithm involves a compromise between accuracy and complexity. The algorithm is successful when $\partial g(\boldsymbol{\theta}^k)/\partial \theta \approx 0$ or when $(\boldsymbol{\theta}^k)$ reaches below a satisfactory near zero threshold in less than K steps, otherwise, the solution diverges or is ambiguous towards the received signal and can't be used.

In the remainder of this section, it is considered that the nonlinearity that models the power amplifier at the transmitter is the SSPA. Under this condition, the equation (4.10) is written as a function of the two parameters of the SSPA and thus vector $\boldsymbol{\theta}$ has two values, namely: saturation level s_M/σ and transition region sharpness p, resulting in

$$\underset{\boldsymbol{\theta}}{\operatorname{argmin}} \left\{ \sum_{n=0}^{N-1} | \frac{|s_n|}{(1 + (\frac{|s_n|}{s_M})^{2p})^{\frac{1}{2p}}} e^{jarg(s_n)} - y_n|^2 \right\}. \tag{4.12}$$

For the following plots, the MATLAB function $lsqcurvefit$ was used to implement the described least squares algorithm.

Figure 4.14 presents the magnitude of the signal before nonlinear distortion on the x-axis and after on the y-axis. The estimated distortion model can be compared to the true model that accurately described the transmitter's PA and to the received signal.

From the figure, it can be noted that the cloud of points associated with the pilot signals allows one to have clear insights into the shape of the function used to model the nonlinear amplifier. Therefore, this suggests that a least square error method can be employed to accurately extract the parameters of the model. This is precisely what is done and the resulting estimated curve of the amplification characteristic is also presented in the figure. As can be observed, the estimated curve is almost equal to the real curve associated with the transmitter PA nonlinearity.

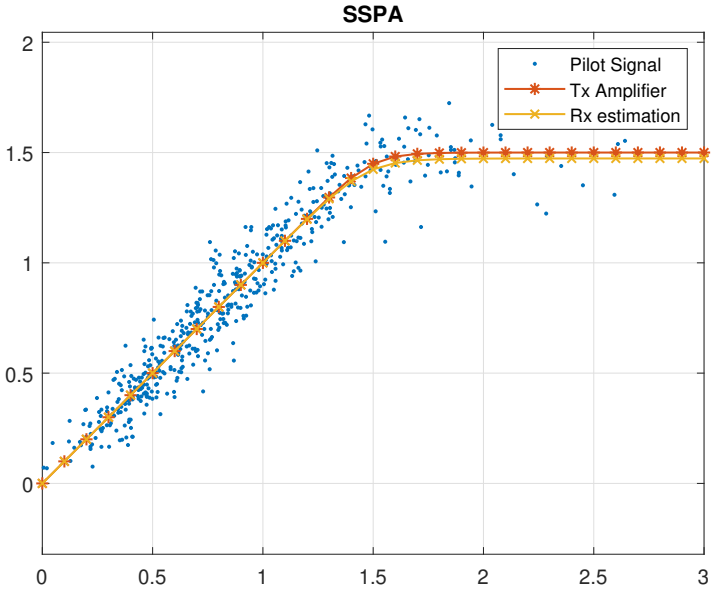

Figure 4.14: Magnitude of a signal before and after the nonlinear amplifier considering $SNR = 20dB$.

As mentioned before, for the SSPA model there are two parameters: one that controls the saturation point and another that defines how smooth the transition from the linear to the saturation region is, and thus the points that weigh on the algorithm are only present at a higher amplitude. Unfortunately, the magnitude of OFDM signals follow a Rayleigh distribution, and at higher amplitude is where there is a lower density of points. Thus for nonlinear distortions with higher levels of saturation this estimation method might not be as effective as it is for scenarios with relatively low distortion values.

The pair of plots in figure 4.15 reveal the convergence of the least square error algorithm as a function of the number of performed iterations. As it can be seen, six iterations are enough for the algorithm to converge. In general, the number of iterations depends on the initial estimate and the number of available useful data points. The estimated parameters might appear to have a considerable offset to the expected ones, but by analyzing figure 4.16, which is using the estimated parameters, one can observe that although the spread of points caused by the low SNR is large, the estimated nonlinear model is accurate.

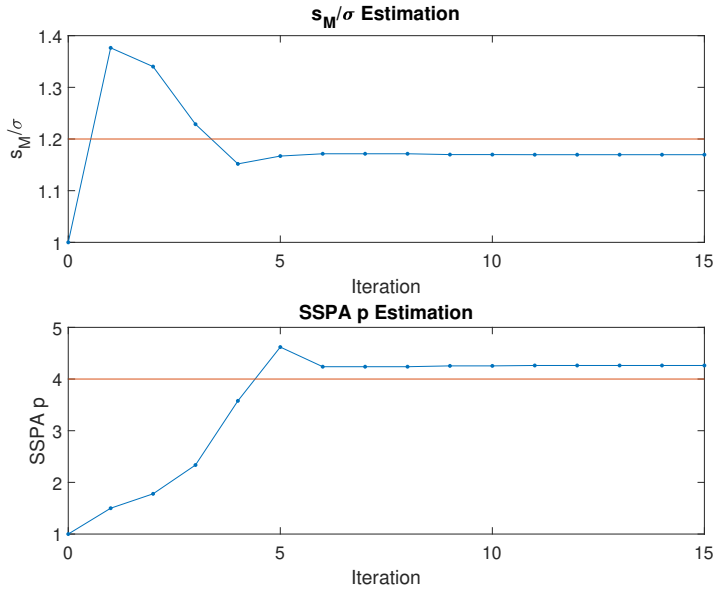

Figure 4.15: Convergence of estimation of parameters. $s_M/\sigma = 1.2$; $SSPAp = 4$; $SNR = 10dB$.

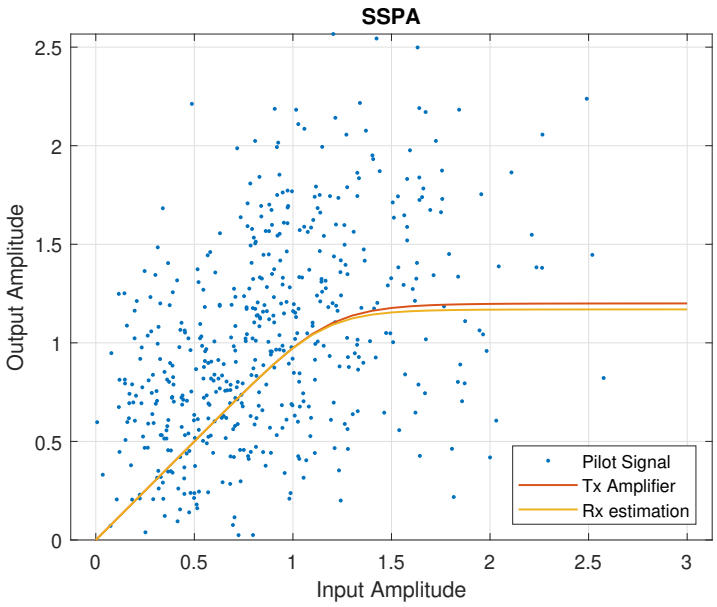

Figure 4.16: Real and estimated amplifier curve from figure 4.15.

In the following, it is considered the normalized mean squared error (NMSE) metric to analyze the sensitivity of nonlinear parameter estimation in a wide range of scenarios. In figure 4.17 the effect of SNR is studied on the NMSE of this estimation method.

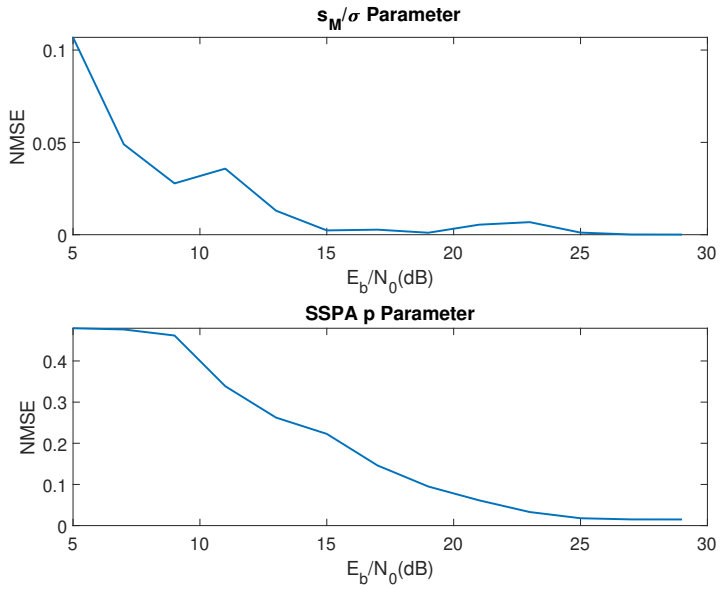

Figure 4.17: NMSE of estimated parameters considering different values of SNR.

As expected, the higher the SNR the smaller the variance of error. The "bumps"on the plots can be explained by the existence of outliers in the data that originate from cases where the curve fitting algorithm diverged. The number of outliers is small (the worst case in the plot is 1% at $5dB$), but their error of the estimated parameters can be enormous. To mitigate this, the outliers are detected if having one of the parameters ten times larger than the expected value and consequently removed from the data. Evidently, the detection of outliers is not strict enough but nevertheless, a clear downward trend is observed.

On previous examples, the estimation of the nonlinearity parameters was done by applying the least square error algorithm for a single OFDM symbol. However, it is interesting to see the effect of considering pilots for the estimation process and to see if this is beneficial in terms of performance.

In Figure 4.18 it is studied the effect of using P symbols in the NMSE of the estimated parameters. The final estimated parameter is the average of the P estimations. From the figure, it can be observed that the algorithm does benefit from using multiple symbols. However, although the gain provided by the second symbol is relatively large, the additional gain of each following symbol decreases.

As already mentioned, this estimation method requires pilot symbols and synchronization between the transmitter and receiver. Figure 4.19 discloses a possible frame design diagram, showing how the P pilot symbols would be placed regularly in between K data symbols during a transmission.

The purpose of the diagram is to clarify that pilot symbols needed for the estimation

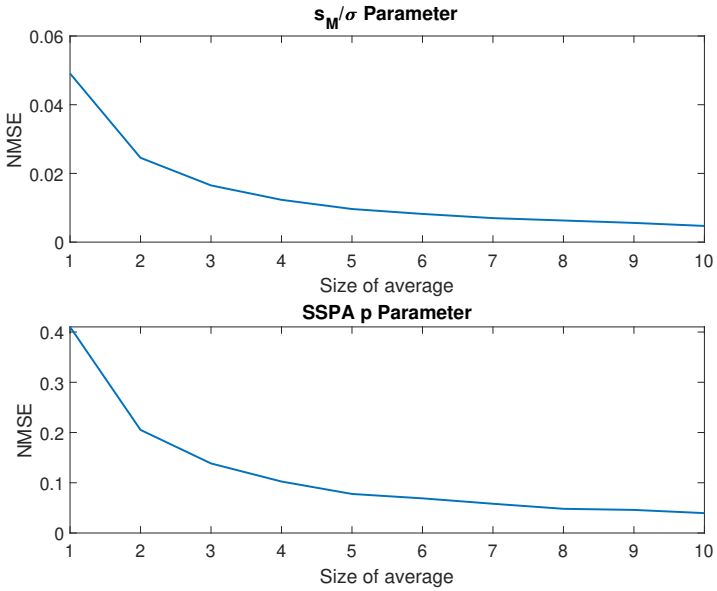

Figure 4.18: Effect of using multiple OFDM symbols to estimate the parameters of an SSPA.

algorithm are sent sequentially with the data and thus are occupying valuable time slots that otherwise would be used for data, making the transmission throughput $K/(P+K)$ times what it could be if only data symbols were transmitted.

Choosing the number P of pilot symbols is a balancing act and involves a tradeoff between performance and data transmission efficiency. On one hand, increasing P improves the accuracy of parameter estimation, leading to a better BER. On the other hand, a large value of P degrades the efficiency ratio $K/(P+K)$. Moreover, it should be noted that the number of P pilot symbols required to achieve a desired estimation accuracy is highly dependent on the characteristics of the OFDM system such as the wireless channel and the amplification characteristic but can be studied with data from plots similar to figure 4.18.

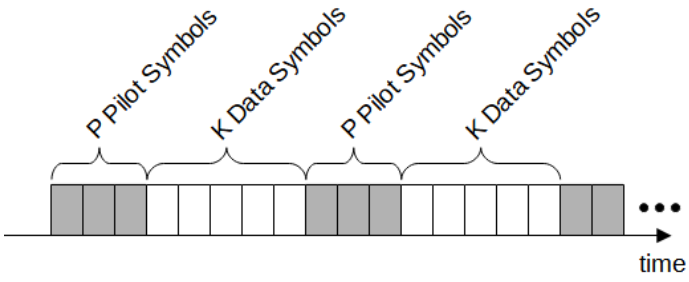

Figure 4.19: Time diagram of a distribution of sequences of pilot symbols in between a stream of data symbols during a transmission.

As previously discussed, the accuracy of the curve fitting estimation method is immensely dependent on the number of points outside the power amplifier's linear region. In figures 4.20 and 4.21 it is presented a scenario with a system identical to the one used

in figure 4.15, but with a higher saturation level and a SNR of 30dB.

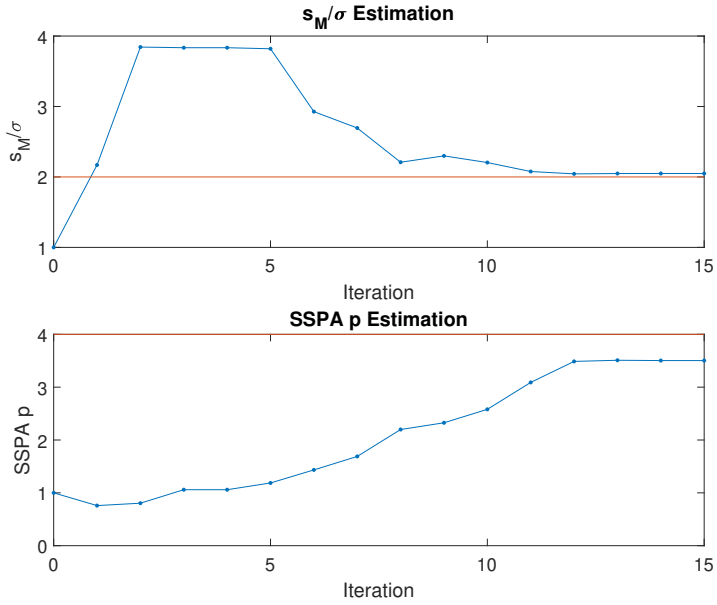

Figure 4.20: Convergence of the estimation process as a function of the number of iterations considering an SSPA with $s_M/\sigma = 2.0$, $p = 4$ and $SNR = 30$ dB.

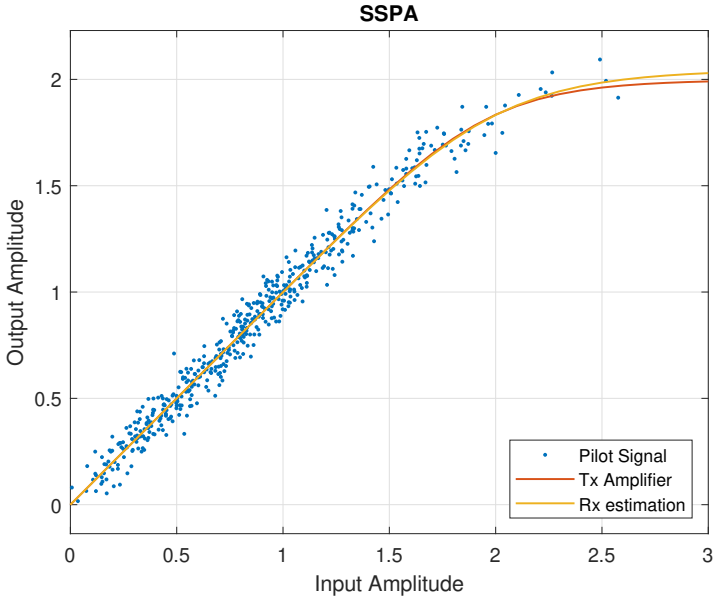

Figure 4.21: Real and estimated amplifier characteristic using the nonlinearity parameters estimated in figure 4.20.

Channel noise is summed to the points but still due to the high SNR the shape of the nonlinear function appears to be discernible. The reality is that due to the relatively very small number of points that are distorted by the nonlinear operation, the ones above a magnitude of around 1.6σ, a wide range of model parameters can generate a curve that appears to be correct. This uncertainty explains why the estimation algorithm needs many more iterations than in the previous scenario, even if in the previous scenarios the

points look much more dispersed. In conclusion, the number of useful points is much more important that the SNR.

All scenarios studied in this section consider 16-QAM OFDM systems with $N = 128$ subcarriers. As it was shown, a saturation level of $s_M/\sigma = 2.0$ does not have a severe effect on BER for a 16-QAM (see figure 4.2), and the distortion characteristic can be accurately estimated because the system has many subcarriers. For a QAM system of higher dimensions or/and with fewer subcarriers, a distortion of $s_M/\sigma = 2.0$ can be much more challenging to estimate. The effects of considering larger constellations are evaluated in the next section.

4.3 Performance of Bussgang Receivers with Estimated Nonlinearity Parameters

In the previous section, two methods to estimate the nonlinearity parameters of the transmitter's power amplifier were studied. In the right conditions, both can achieve a fairly high level of accuracy. However, there is always an error since the estimation is never exact. In this section, we'll study the effect of a mismatch between the real power amplifier characteristic at the transmitter and the estimated model at the receiver. This study is important for analyzing the performance of Bussgang receivers in practical scenarios where the nonlinearity characteristic is not available.

Figure 4.22 shows the block diagram of an OFDM system with a receiver that estimates the distortion component of the original signal using an estimated (and mismatched) nonlinear characteristic. This test bench can give a glimpse of the effect of the mismatch on a scenario where the whole system except the nonlinear parameters is ideal.

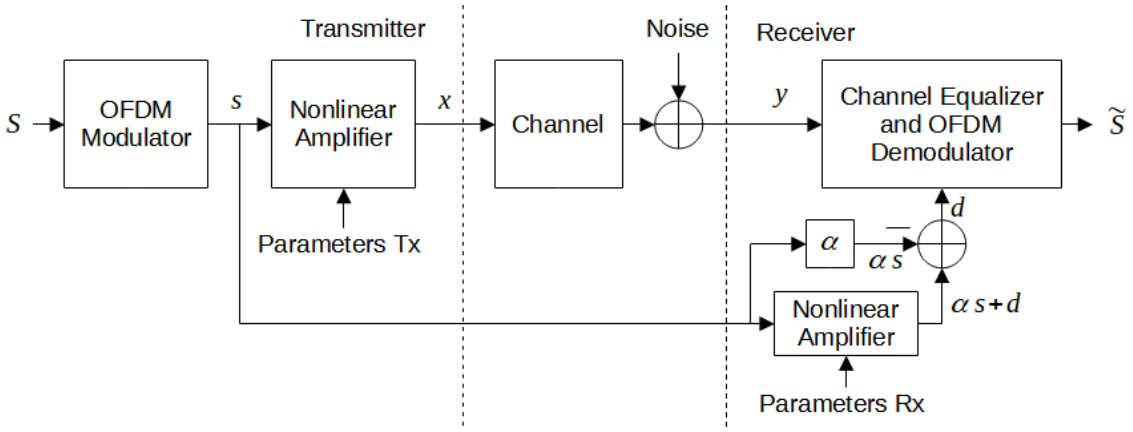

Figure 4.22: Block diagram of a system where the distortion component available to the receiver is mismatched with the received signal.

Figure 4.23 shows the effect of mismatch of nonlinearity parameters on the BER floor using the system depicted in 4.22.

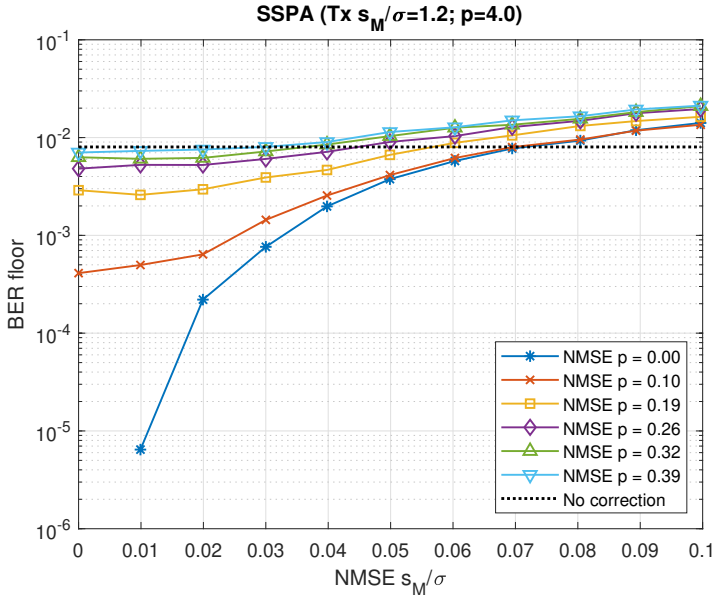

Figure 4.23: BER floor when mismatched nonlinear distortion is available to the receiver.

It should be noted that the distortion component of a parallel and mismatched model is subtracted from the received signal. Thus there is the possibility of error propagation to the final estimated signal.

The effect of saturation level s_M/σ mismatch is observed in the horizontal axis where it can be noted that for larger variations, on the right side, the BER floor increases. Notice that although the NMSE reaches 0.1, a more realistic estimation of saturation level can easily achieve NMSE lower than 0.01 as is observed in figures 4.17 and 4.18. In that region, the plots present an insignificantly small slope which means that in these conditions, the effect of the mismatch of saturation level is insignificant. On the other hand, it can be observed the smoothness parameter p of the SSPA has an enormous effect on the BER floor for the left region. This result is unexpected, given that the p parameter only affects the harshness of the power amplifier's transition from the linear to the saturation region and only a small number of points in the signal, which have magnitude at the transition region, are affected by the p parameter. This is also the reason why the estimation of that parameter has much larger variations than that of the saturation level.

In the plot there is also a line labeled as "No correction", this is the BER level for an OFDM system that doesn't do any kind of correction, i.e. with the conventional receiver of figure 4.1. This curve sets a limit where not doing any distortion component estimation at all is better than using the estimated nonlinearity parameters and as expected if the mismatch is too large then the performance of the system can be substantially degraded due to error propagation effects.

The block diagram in figure 4.24 is an OFDM system where a BNC receiver estimates the received signal while using a mismatched model of the nonlinear amplifier. In this case the receiver has no additional information about the transmitted signal, which makes it a realistic scenario.

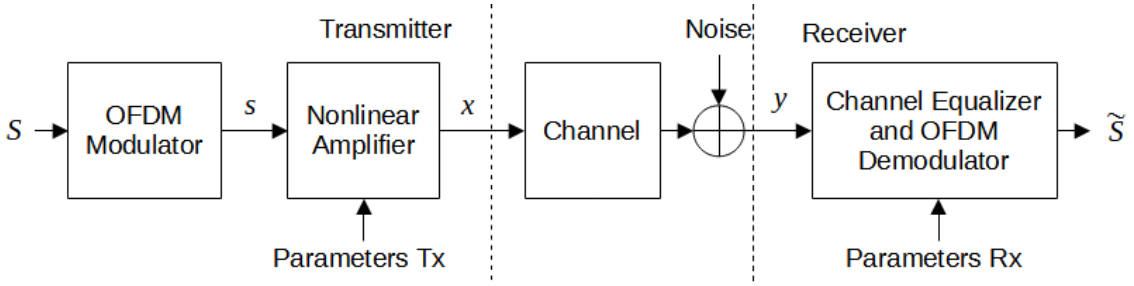

Figure 4.24: Block diagram of a system where the model parameters from the nonlinear amplifier are mismatched.

The effect of the mismatch of nonlinearity parameters on the BER floor using an OFDM system with a BNC receiver is found in figure 4.25.

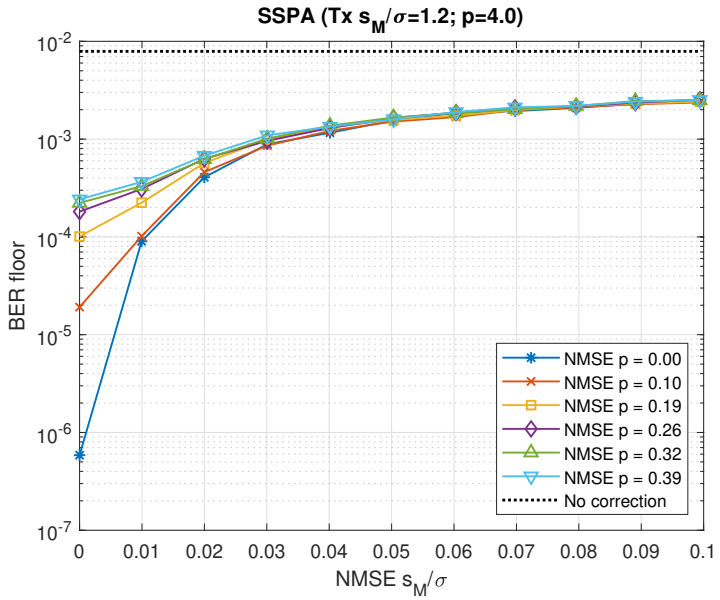

Figure 4.25: Evolution of the BER floor when mismatched nonlinearity parameters are used in a BNC receiver.

From the figure, what is striking is that the BNC algorithm appears to completely nullify the effect of the mismatch of the SSPA p parameter after NMSE $s_M/\sigma > 0.03$, which has the largest weight on the degradation on the previous system depicted in figure 4.22. On top of that, BNC also makes the system robust against extremely large variations of the saturation level. This unexpectedly better performance of BNC when compared with the use of a distortion component with mismatched parameters is a good surprise and shows that it is always beneficial to use BNC even if the estimation of nonlinearity parameters is imprecise.

Until this moment, all presented simulations considered 16-QAM systems, which are the smallest QAM constellations that can experience severe degradation by nonlinear distortion from the shrinkage of the constellation of the linear factor α of the Bussgang's

theorem, as seen in section 3.2.2. These simulations were done with the hope that the findings can be extended to higher constellation sizes to some degree, namely that nonlinear OFDM systems greatly benefit from having a BNC receiver even if the nonlinear model used is mismatched with the power amplifier. In this section, it is verified if previous conclusions can be applied to 1024-QAM systems, which are in the realm of super-QAM scenarios desired for upcoming 6G systems.

Figure 4.26 presents the BER curves for a nonlinear 1024-QAM system with a traditional receiver. Multiple plots are shown, each one with a different saturation level s_M/σ for the SEL model of the power amplifier. As expected, all plots follow the BER curve of the linear system, i.e. the dotted line, until they diverge into a BER floor. However, it is important to note that the saturation levels used in this figure ($s_M/\sigma > 2.0$) would lead to relatively low distortion levels in a 16-QAM scenario and consequently very low BER floor (see figure 4.2), but with 1024-QAM the impact is enormous and for saturation levels lower than $s_M/\sigma = 2.0$, the BER is almost a straight line. In these scenarios the distortion is intolerable and communication cannot take place.

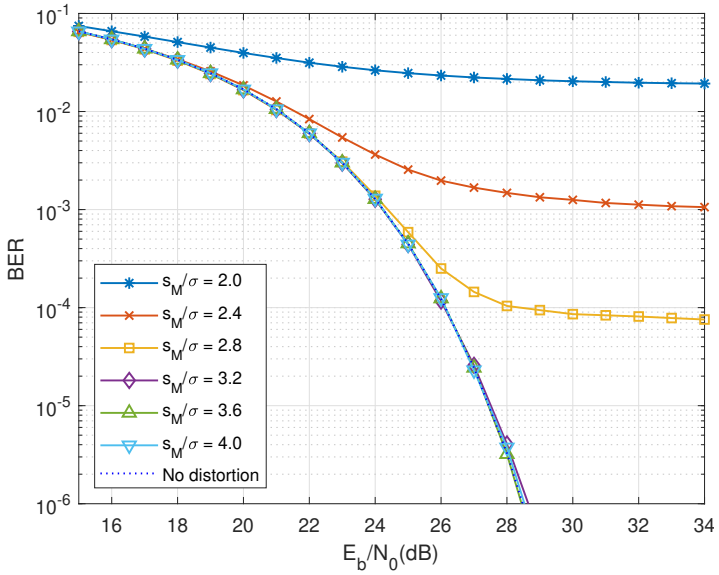

Figure 4.26: Impact of a SEL amplifier on BER for a 1024-QAM system.

In fact, the tendency for higher BER floors at the same saturation level with the increase of constellation size can be verified in figure 4.27.

For example, a BER floor of 10^{-2} is achieved approximately at $s_M/\sigma = 1.2$ for 16-QAM, at $s_M/\sigma = 1.8$ for 256-QAM and approximately at $s_M/\sigma = 2.3$ for 4096-QAM even though that by increasing the saturation level the effect of the nonlinear distortion is lessened and eventually will get to the point that the PAPR of most transmitted symbols is below s_M/σ (thus don't experience any distortion). However, because the BER floor is still 10^{-2}, it means that the symbols affected by the slight clipping are completely unrecoverable by the traditional receiver.

Continuing this thought, for 1024-QAM to achieve a reasonable BER, it is required a

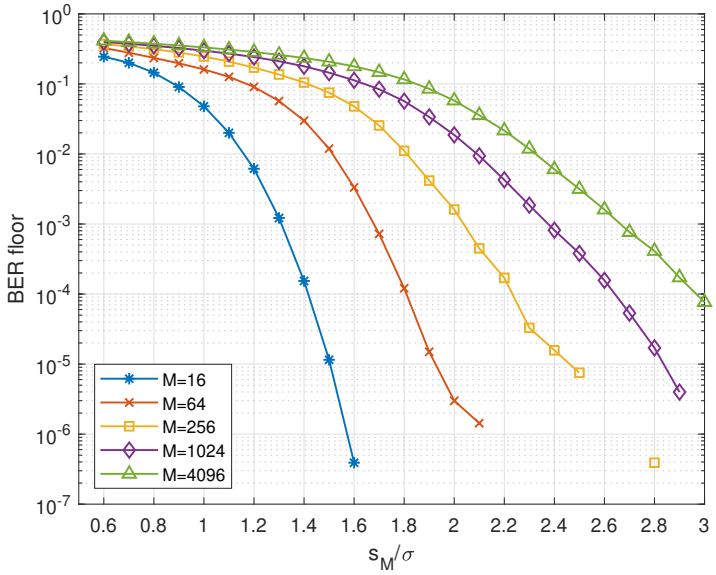

Figure 4.27: Comparison of BER floor between constellation sizes as a function of saturation level s_M/σ.

high clipping level, which results in a minor nonlinear distortion effect and thus a mostly nil Bussgang's distortion component. In this case we would expect that employing a BNC receiver would achieve perfect results, given that the BNC algorithm only has to estimate the very small part of the signal that is affected by distortion, however this is not the case. Figure 4.28 shows the BER plots of a 1024-QAM nonlinear OFDM system with a BNC receiver and can be directly compared with figure 4.26.

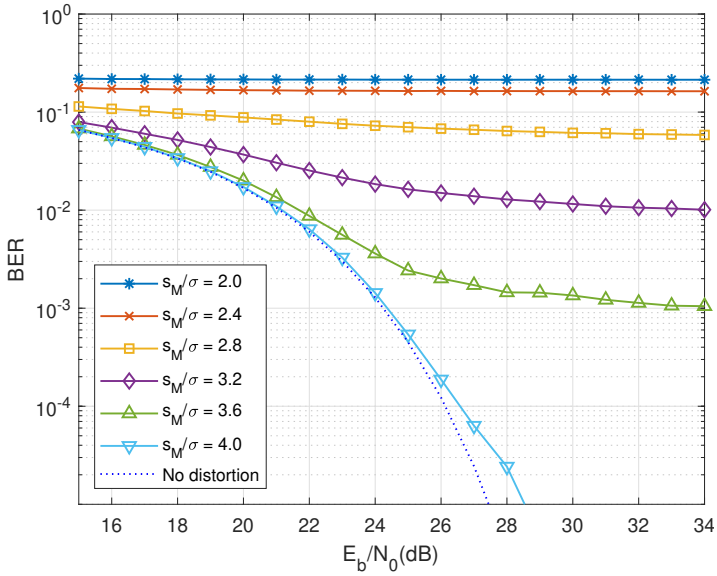

Figure 4.28: BER performance of a 4-iteration BNC receiver considering a nonlinear OFDM system 1024-QAM constellations.

It can be seen that not only the BNC receiver is unable to estimate the distortion component, but also extremely degrades the BER that a conventional receiver could achieve. It is not shown in the figure plots for stronger saturation levels, however, the same results

were observed for other clipping levels, i.e. no improvements were observed. Therefore, for the considered scenarios it can be concluded that BNC receivers are not applicable with Super-QAM systems.

After the revelation of the nonperforming BNC receiver with Super-QAM systems, an interesting topic to research is understanding why it behaves so well on 16-QAM but not on higher constellations. To this end, a few 1024-QAM OFDM symbols were studied and the pair of figures 4.29 and 4.30 show the magnitude and complex amplitude of one of these symbols. This symbol was chosen at random and presents the same characteristics seen on all other studied symbols.

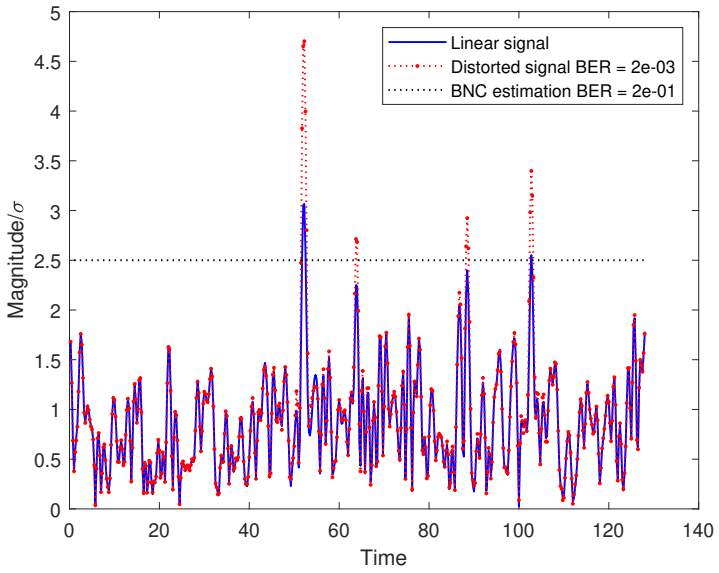

Figure 4.29: Effect of the BNC algorithm on the magnitude of a 1024-QAM symbol. $SNR = 30dB$.

The magnitude plot displays the symbol at three stages: the original ”linear”symbol, the symbol distorted by the nonlinear amplifier which is also the transmitted symbol, and the BNC estimation. At the second stage, only the clipping threshold of the distorted symbol is shown because its plot is the same as the linear one but with magnitude clipped at $2.5/\sigma$. One glaring characteristic of the BNC estimation is the pronounced overestimation of the clipped peaks and growth of peaks in the linear region near the threshold, the rest of the signal appears to not experience any significant transformation. This minority of points that are touched by the BNC algorithm may seem too small to be of significance but the BER metric says otherwise, the slight clipping of the symbol is enough to set a BER of 2 in 1000 but the BNC brings that number up to 2 in 10. In other words, the BER becomes a hundred times worse.

Figure 4.30 shows the complex amplitudes of the subcarriers of the same symbol.

It shows all the points of a 1024-QAM constellation, the 128 OFDM subcarrier complex amplitudes of the linear symbol, and the displacement of those complex amplitudes as a result of the BNC estimation. Looking at the position of the points after the displacement makes it easy to understand why the resulting BER is so bad. For each displaced point, the

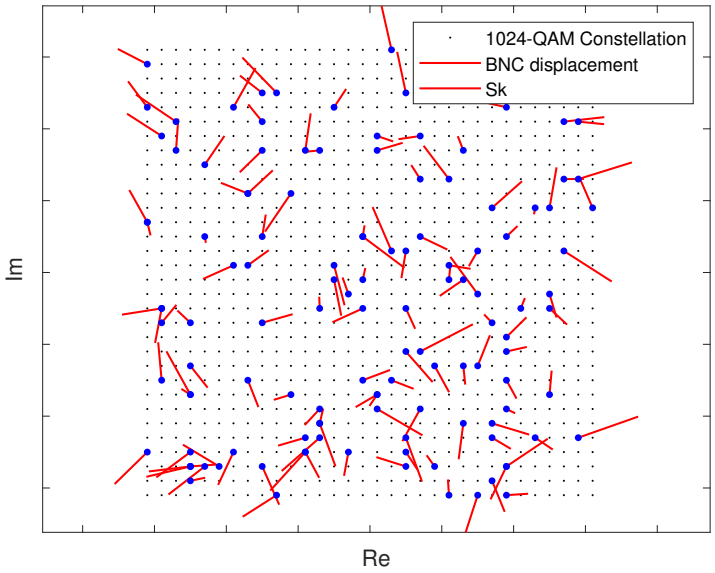

Figure 4.30: Effect of the BNC algorithm on the complex amplitude of the same symbol of figure 4.29.

hard decision modulator chooses the nearest constellation point as the final data point, and the issue is that for 1024-QAM most displacement vectors end up at the areas of neighboring constellation points. One important remark that has to be made is that these displacement vectors are related to the power of the distortion component from Bussgang's theorem and thus their relative magnitude is dependent on the nonlinear model and not on the size of the constellation. The reason why BER works for 16-QAM is that its 4×4 constellation is much less dense than the 32×32 from 1024-QAM, while the displacement vectors have the same relative size. Therefore, for 16-QAM, the displacement usually doesn't reach a neighbor.

Despite the obviously incorrect estimation in figure 4.30, the BNC estimation in figure 4.29 accurately describes the region below the clipping level. Therefore, it can be concluded that not knowing the exact magnitude of the region above the clipping level (even if there are only very few and isolated points) makes the symbol ambiguous, in the sense that many valid symbols can express a similar signal on the linear region, and thus the BNC estimation ends up choosing one of these possible symbols randomly. For 16-QAM systems, the smaller constellation limits the number of possible symbols but for bigger constellations the number of possible symbols is much larger.

5

Conclusions and Future Work

5.1 Conclusions

In this work, the OFDM performance degradation due to nonlinear effects of the transmitter's PA and methods to mitigate those effects were studied, both for systems with small constellations as well as for the so-called super-QAM.

In chapter 2 were presented several state-of-the-art techniques employed in the receiver to lessen the effects of the nonlinear distortion. From those techniques, three main approaches were discerned. The first approach is to simply accept distortion as part of the channel noise and employ a conventional receiver based on a simple hard decision operation. The second approach is to estimate the distortion component of the signal, remove it from the received signal and thus rebuild the original linear signal. The third approach is to consider the PA's nonlinear effect as a legitimate stage of the signal modulation and thus the receiver's estimation of the signal consists of the identification of the signal just as it is, namely by considering that the nonlinear distortion term has useful information on the transmitted data. It was demonstrated that each of these techniques usually gives rise to a strong tradeoff between performance and complexity. The aforementioned receivers were introduced and their algorithms were briefly described. In addition, several BER performance results were presented.

In chapter 3, OFDM was introduced with emphasis to the analysis of nonlinear distortion effects. OFDM system was characterized with its benefits highlighted, namely the high spectral efficiency and simple channel equalization. It was also demonstrated that OFDM signals are prone to nonlinear effects due to their Rayleigh distributed envelope and therefore present a very high PAPR. Several models to describe the nonlinear distortion were presented and it was shown that according to Bussgang's theorem, the nonlinearly distorted signal can be decomposed into a linear and an uncorrelated component. Super-QAM OFDM systems were introduced and it was observed that the nonlinear effects on systems with larger constellations are much more severe since even considerable low distortion levels can have a tremendous impact on super-QAM systems. In order to compare levels of distortion between symbols or systems affected by nonlinear effects,

metrics for measuring PAPR and quantifying the constellation spread such as the EVM were presented.

In chapter 4, OFDM systems with BNC receiver were studied in detail. This type of receiver estimates the distortion component of the nonlinearly distorted signal and subtracts it from the received signal, resulting in what is believed to be the original linear signal. BNC receiver was compared with the conventional receiver and a theoretical receiver that knows the true distortion component. It is observed that for 16-QAM systems, the BNC greatly improves the BER curve when compared with the conventional receiver. As expected, for the theoretical receiver the performance is as if there was no distortion at all, although there is always a loss in the SNR caused by the transmission of the distortion term. It was seen that to employ a BNC receiver in practical scenarios, it is required to have a model of the distortion operation that the signal experiences in the transmitter. In order to do that, two methods to estimate the parameters of nonlinearity models were studied, namely: a PDF-based algorithm which extracts model parameters from PDF or histogram of the signal, and least squares curve fitting method that with the support of pilot signals can minimize the error between any model and the received pilots. This latter algorithm for estimating the nonlinearity parameters was studied in detail through an NMSE analysis of the impact of variations of SNR, the number of iterations, and the number of pilots. This allowed to study its robustness under different transmission scenarios. The performance of Bussgang receivers using the estimated parameters was presented, being shown that this performance is closely related to the quality of the estimated parameters. Finally, it was concluded that employing a BNC receiver in a super-QAM system might result in a worse BER curve than if using the conventional receiver, and an explanation for that phenomenon was given.

5.2 Future Work

In relation to future work, interesting research directions are as follows:

- Consider an analytical relation between the data-to-pilot symbol ratio regarding the estimation of nonlinearity parameters (i.e., the frame design aspects) and analyze the corresponding system's performance.
- A method to obtain pilot symbols that in the time domain present a high density of points on the transition between the linear and nonlinear regions of the PA could greatly improve the curve fitting parameter estimation.
- Modifying the BNC receiver so that it can prioritize the smallest changes possible on the received symbol's constellation would be immensely beneficial for super-QAM constellations.

Bibliography

[1] J. M. Lourenço. The NOVAthesis LaTeX Template User's Manual. NOVA University Lisbon. 2021. url: https://github.com/joaomlourenco/novathesis/raw/master/template.pdf (cit. on p. ii).

[2] A. Dogra, R. K. Jha, and S. Jain. "A Survey on Beyond 5G Network With the Advent of 6G: Architecture and Emerging Technologies". In: IEEE Access 9 (2021), pp. 67512–67547. doi: 10.1109/ACCESS.2020.3031234 (cit. on pp. 1–3, 27).

[3] C. Deng et al. "IEEE 802.11be Wi-Fi 7: New Challenges and Opportunities". In: IEEE Communications Surveys & Tutorials 22.4 (2020), pp. 2136–2166. doi: 10.1109/COMST.2020.3012715 (cit. on pp. 1, 2).

[4] M. Giordani et al. "Toward 6G Networks: Use Cases and Technologies". In: IEEE Communications Magazine 58.3 (2020), pp. 55–61. doi: 10.1109/MCOM.001.1900411 (cit. on p. 1).

[5] B. Sklar. "Rayleigh fading channels in mobile digital communication systems. I. Characterization". In: IEEE Communications Magazine 35.9 (1997), pp. 136–146. doi: 10.1109/35.620535 (cit. on p. 2).

[6] T. Huang et al. "A Survey on Green 6G Network: Architecture and Technologies". In: IEEE Access 7 (2019), pp. 175758–175768. doi: 10.1109/ACCESS.2019.2957648 (cit. on p. 2).

[7] J. Joung, C. K. Ho, and S. Sun. "Spectral Efficiency and Energy Efficiency of OFDM Systems: Impact of Power Amplifiers and Countermeasures". In: IEEE Journal on Selected Areas in Communications 32.2 (2014), pp. 208–220. doi: 10.1109/JSAC.2014.141203 (cit. on pp. 2, 3).

[8] J. Yang et al. "A Compensation Method for Nonlinear Distortion in OFDM System". In: The 9th International Conference on Advanced Communication Technology. Vol. 2. 2007, pp. 881–884. doi: 10.1109/ICACT.2007.358501 (cit. on pp. 3, 19).

[9] J. Urban and R. Marsalek. “PAPR Reduction by Combination of Interleaving with Repeated Clipping and Filtering in OFDM”. In: 2007 17th International Conference Radioelektronika. 2007, pp. 1–4. doi: 10.1109/RADIOELEK.2007.371658 (cit. on pp. 3, 28).

[10] O. Chandrakar et al. “Reduction of the nonlinearities by decreasing Peak to Average Power Ratio (PAPR) for Coherent Optical OFDM-WDM system using Exponential Compading”. In: 2015 IEEE UP Section Conference on Electrical Computer and Electronics (UPCON). 2015, pp. 1–4. doi: 10.1109/UPCON.2015.7456705 (cit. on p. 3).

[11] N. Sharan, S. Ghorai, and A. Kumar. “Peak-to-Average Power Ratio (PAPR) Reduction Using Combination of Precoding and Companding Techniques for VLC OFDM Systems”. In: 2019 TEQIP III Sponsored International Conference on Microwave Integrated Circuits, Photonics and Wireless Networks (IMICPW). 2019, pp. 149–153. doi: 10.1109/IMICPW.2019.8933194 (cit. on pp. 3, 26).

[12] N. Bibi and B. Cheetham. “Clipping noise mitigating iterative receivers for OFDM”. In: 2012 IEEE 3rd International Conference on Networked Embedded Systems for Every Application (NESEA). 2012, pp. 1–5. doi: 10.1109/NESEA.2012.6474024 (cit. on pp. 3, 7, 8, 18, 19).

[13] J. L. Guerreiro, R. Dinis, and P. Montezuma. “On the optimum multicarrier performance with memoryless nonlinearities”. In: IEEE Transactions on Vehicular Technology (2014), pp. 1–1. doi: 10.1109/TVT.2014.2381874 (cit. on p. 3).

[14] J. Guerreiro et al. “On the Achievable Performance of Nonlinear MIMO Systems”. In: IEEE Communications Letters 23.10 (2019), pp. 1725–1729. doi: 10.1109/LCOMM.2019.2929040 (cit. on p. 3).

[15] H. E. Rowe. “Memoryless nonlinearities with Gaussian inputs: Elementary results”. In: The Bell System Technical Journal 61.7 (1982), pp. 1519–1525. doi: 10.1002/j.1538-7305.1982.tb04356.x (cit. on pp. 6, 20).

[16] S. V. Zhidkov and R. Dinis. “Belief Propagation Receivers for Near-Optimal Detection of Nonlinearly Distorted OFDM Signals”. In: 2019 IEEE 89th Vehicular Technology Conference (VTC2019-Spring). 2019, pp. 1–6. doi: 10.1109/VTCSpring.2019.8746319 (cit. on pp. 7, 12–14).

[17] H. Bouhadda et al. “Receiver Technique for Detection and Correction of Nonlinear High Power Amplifier Distortion Errors in OFDM Systems”. In: 2015 IEEE 81st Vehicular Technology Conference (VTC Spring). 2015, pp. 1–5. doi: 10.1109/VTCSpring.2015.7146044 (cit. on pp. 8, 10).

[18] J. Guerreiro, R. Dinis, and P. Montezuma. “Optimum and Sub-Optimum Receivers for OFDM Signals with Strong Nonlinear Distortion Effects”. In: IEEE Transactions on Communications 61.9 (2013), pp. 3830–3840. doi: 10.1109/TCOMM.2013.072913.120344 (cit. on pp. 9–13).

[19] J. M. B. Oliveira, M. R. D. Rodrigues, and H. M. Salgado. "Optimum Receivers for Non-Linear Distortion Compensation of OFDM Signals in Fiber Supported Wireless Applications". In: Microwave Photonics, 2007 Interntional Topical Meeting on. 2007, pp. 120–123. doi: 10.1109/MWP.2007.4378151 (cit. on p. 11).

[20] S. V. Zhidkov. Detection of Nonlinearly Distorted OFDM Signals via Generalized Approximate Message Passing. 2017. doi: 10.48550/ARXIV.1703.01562. url: https://arxiv.org/abs/1703.01562 (cit. on p. 13).

[21] J. Tubbax et al. "OFDM versus Single Carrier with Cyclic Prefix: a system-based comparison". In: IEEE 54th Vehicular Technology Conference. VTC Fall 2001. Proceedings (Cat. No.01CH37211). Vol. 2. 2001, 1115–1119 vol.2. doi: 10.1109/VTC.2001.956948 (cit. on p. 16).

[22] Q. Lu, L. Gui, and X.-Z. Fang. "A New Scheme to Mitigate the OFDM High PAR Problem by Minimizing the Signal's Nonlinear Distortion Caused by HPA". In: IEEE Transactions on Broadcasting 52.4 (2006), pp. 576–578. doi: 10.1109/TBC.2006.884733 (cit. on p. 19).

[23] B. Goebel et al. "PAPR reduction techniques for coherent optical OFDM transmission". In: 2009 11th International Conference on Transparent Optical Networks. 2009, pp. 1–4. doi: 10.1109/ICTON.2009.5184979 (cit. on pp. 22, 26, 28).

[24] S. Ramavath and R. S. Kshetrimayum. "Analytical calculations of CCDF for some common PAPR reduction techniques in OFDM systems". In: 2012 International Conference on Communications, Devices and Intelligent Systems (CODIS). 2012, pp. 393–396. doi: 10.1109/CODIS.2012.6422221 (cit. on p. 24).

[25] T. Jiang et al. "Derivation of PAPR Distribution for OFDM Wireless Systems Based on Extreme Value Theory". In: IEEE Transactions on Wireless Communications 7.4 (2008), pp. 1298–1305. doi: 10.1109/TWC.2008.060862 (cit. on p. 24).

[26] K. Anoh, C. Tanriover, and B. Adebisi. "On the Optimization of Iterative Clipping and Filtering for PAPR Reduction in OFDM Systems". In: IEEE Access 5 (2017), pp. 12004–12013. doi: 10.1109/ACCESS.2017.2711533 (cit. on p. 25).

[27] Z. Feng et al. "Analysis on the Definition Consistency Problem of EVM Measurement and its Solution". In: IEEE Transactions on Instrumentation and Measurement 69.2 (2020), pp. 528–532. doi: 10.1109/TIM.2019.2901561 (cit. on p. 27).

[28] C. Zhao and R. J. Baxley. "Error Vector Magnitude Analysis for OFDM Systems". In: 2006 Fortieth Asilomar Conference on Signals, Systems and Computers. 2006, pp. 1830–1834. doi: 10.1109/ACSSC.2006.355078 (cit. on p. 27).

[29] S. Ruder. An overview of gradient descent optimization algorithms. 2017. arXiv: 1609.04747 [cs.LG] (cit. on p. 40).